NUREG/CR-6114
Vol. 3

Performance Assessment of a Hypothetical Low-Level Waste Facility

Groundwater Flow and Transport Simulation

Prepared by
M. E. Talbott, L. W. Gelhar

Department of Civil and Environmental Engineering
Massachusetts Institute of Technology

Prepared for
U.S. Nuclear Regulatory Commission

NUREG/CR-6114
Vol. 3

Performance Assessment of a Hypothetical Low-Level Waste Facility

Groundwater Flow and Transport Simulation

Manuscript Completed: December 1993
Date Published: May 1994

Prepared by
M. E. Talbott, L. W. Gelhar

T. J. Nicholson, NRC Project Manager

Ralph M. Parsons Laboratory
Department of Civil and Environmental Engineering
Massachusetts Institute of Technology
Cambridge, MA 02139

Prepared for
Division of Regulatory Applications
Office of Nuclear Regulatory Research
U.S. Nuclear Regulatory Commission
Washington, DC 20555-0001
NRC FIN D2044

ABSTRACT

Stochastic subsurface hydrologic theory is applied to data for a hypothetical low-level radioactive waste site to demonstrate the features of the hydraulic parameter estimation process, as developed by Gelhar and others. Effective values of hydraulic conductivity, macrodispersivity, and macrodispersivity enhancement are estimated from the data in this manner. A two-dimensional saturated flow and transport finite-element computer code is used to model the site. Four different isotope inputs and two types of input configurations contribute to an evaluation of model sensitivities. These sensitivities of the mean concentrations and the uncertainties around the mean are explored using an analytical model as an example. Results indicate that the spatial heterogeneity of isotope sorption, through its contribution to longitudinal dispersivity enhancement, has a large effect on the magnitude of concentration predictions, especially for isotopes with short half-lives in comparison to their retarded mean travel times. This observation emphasizes the need for accurate site data measurements that compliment the parameter estimation process. A comparison of simplified analytical screening models with the numerical model predictions shows that the analytical models tend to underestimate concentration levels at low times, potentially as a result of oversimplification of the flow field. Future models could address aspects that are neglected in this report, such as three-dimensionality or unsaturated flow and transport.

TABLE OF CONTENTS

page

Abstract iii

List of Figures vii

List of Tables xi

Executive summary xiii

Foreword xv

Acknowledgements xvii

Abbreviations xix

Chapter 1: Introduction 1

Chapter 2: Site Characteristics 3

2.1 General Description 3

2.2 Site Geology and Hydrology 3

Chapter 3: Parameter Estimation 5

3.1 Sources of Data 5

3.2 Saturated Zone 5

3.2.1 Correlation Scales 7

3.2.2 Hydraulic Conductivity 7

3.2.3 Macrodispersivity 9

3.2.4 Longitudinal Macrodispersivity Enhancement through Sorption Variability 12

3.3 Unsaturated Zone 14

Chapter 4: Isotope Characteristics 19

4.1 Screening Process 19

4.1.1 Step Input 21

4.1.2 Pulse Input 22

4.2 Sorption Dependence and Evaluation 24

4.2.1 Strontium-90: Sorption Dependence on pH 24

4.2.2 Technetium-99: Sorption Dependence on Clay Content 27

4.2.3 Uranium-238: Macrodispersivity Enhancement 30

4.3 Discussion 30

Chapter 5: Numerical Models 31

5.1 Rectangular Model 31

5.1.1 Model Configuration 31

5.1.2 Results 33

5.1.3 Discussion and Sensitivity Analysis 45

TABLE OF CONTENTS
(continued)

page

5.2 Radial Model 45
5.2.1 Model Configuration 47
5.2.2 Results 49
5.2.3 Discussion 52
5.3 Predictions and Uncertainty 52
5.3.1 Analytical Predictions of Numerical Results 52
5.3.2 Uncertainties in Model Predictions 56
Chapter 6: Conclusions and Recommendations 61
6.1 Conclusions 61
6.2 Recommendations 62
References 63
Appendix A: One-dimensional Step Input Solution 65
Appendix B: Two-dimensional Pulse Input Solution 67

LIST OF FIGURES

page

Figure 2-1 Map of hypothetical LLW site showing water table contours, relative scale, and proximity to spring and city. 4

Figure 3-1 Collected values of hydraulic conductivity versus depth. From laboratory tests on soil samples from seven wells, on-site slug tests, an aquifer test, and specific capacity of a local city well. 6

Figure 3-2 Histogram showing distribution of thickness of clay lenses for nineteen observations from well-drilling logs. 8

Figure 3-3 Horizontal correlation scale of hydraulic conductivity, λ_1, as compared to overall problem scale. 8

Figure 3-4 Standard deviation of hydraulic conductivity, σ_{lnK}, as compared to overall problem scale for a collection of site examples 10

Figure 3-5 Graph showing relationship of K_G and σ_{lnK} for each zone to compilation of hydraulic conductivity data. 11

Figure 3-6 Graph showing relationship of K_{11} and K_{33} for each zone to compilation of hydraulic conductivity data. 11

Figure 3-7 Longitudinal macrodispersivity versus overall problem scale with data classified by reliability. 13

Figure 3-8 Relationship between R and lnK showing correlation factor, ζ, and residual, η. 15

Figure 3-9 Idealized representation of the unsaturated zone in cross-section at the hypothetical site, showing distance from bottom of trench to water table. 17

Figure 4-1 Collected values of pH versus depth. 25

Figure 4-2 Distribution of measured pH values from 95 site water and soil samples. 26

Figure 4-3 Relationship of site pH variation to strontium-90 K_d. 26

Figure 4-4 Distribution of measured values of clay content from 14 site soil samples. 29

Figure 4-5 Relationship of site clay content variation to technetium-99 K_d. 29

Figure 5-1 Cross section of 2D rectangular model showing relative thickness of zones. 32

page

Figure 5-2 Mesh and no-flow and fixed-head boundary conditions used in 2D rectangular finite element model. 34

Figure 5-3 Lines of constant head for equal head drops for the 2D anisotropic rectangular model. 35

Figure 5-4 Flow pattern for 2D rectangular model with velocity vectors at center of elements. Arrows at downstream boundary indicate flow towards, not flow through impermeable boundary. 35

Figure 5-5 Comparison of concentration breakthrough curves for H-3 at spring and at property boundary well. 37

Figure 5-6 Concentration contours of tritium at a) 50 and b) 150 years. 38

Figure 5-7 Comparison of concentration breakthrough curves for U-238 at spring and at property boundary well. 39

Figure 5-8 Concentration contours of uranium-238 at a) 11300 and b) 14000 years. 40

Figure 5-9 Comparison of concentration breakthrough curves for Sr-90 at spring and at property boundary well. 41

Figure 5-10 Concentration contours of strontium-90 at a) 50 and b) 315 years. 42

Figure 5-11 Comparison of concentration breakthrough curves for Tc-99 at spring and at property boundary well. 43

Figure 5-12 Concentration contours of technetium-99 at a) 20 and b) 300 years. 44

Figure 5-13 Comparison of Sr-90 concentration at the spring for numerical simulations of the 2D rectangular model with A_{11} = 242 m and with A_{11} = 25 m. 46

Figure 5-14 Cross-section of the 2D radial model, showing relative thickness of zones and locations of river, pumping well, and property boundary well. 48

Figure 5-15 Breakthrough concentration curve for tritium at the property boundary well using the 2D radial model. 50

Figure 5-16 Breakthrough concentration curves for tritium at the river and at the pumping well using the 2D radial model. 50

Figure 5-17 Concentration contours of tritium in the 2D radial model cross-section at 605 years. 51

Figure 5-18 Comparison of H-3 concentration breakthrough curves at the spring for the 1D step model prediction and for the 2D rectangular numerical simulation. 53

Figure 5-19 Comparison of U-238 concentration breakthrough curves at the spring for the 1D step model prediction and for the 2D rectangular numerical simulation. 53

page

Figure 5-20 Comparison of Sr-90 concentration breakthrough curves at the spring for the 2D pulse model prediction and for the 2D rectangular numerical simulation. 55

Figure 5-21 Comparison of Tc-99 concentration breakthrough curves at the spring for the 2D pulse model prediction and for the 2D rectangular numerical simulation. 55

Figure 5-22 Sensitivity of the 2D pulse screening model for strontium-90 to changes in input parameters. 57

Figure 5-23 Mean concentration and plus two standard deviations for strontium-90 at the spring, using the 2D pulse screening model. 59

LIST OF TABLES

page

Table 3-1 Summary of hydraulic parameters. 10

Table 4.1 Isotopes of potential interest in modeling. 20

Table 4.2 Summary of parameters for step input screening model. 23

Table 4.3 Summary of parameters for pulse input screening model. 23

Table 4.4 Parameters used to calculate effect of Strontium-90 K_d variability. 28

Table 4.5 Parameters used to calculate effect of Technetium-99 K_d variability. 28

Table 4.6 Summary of isotope parameters that are used in the numerical model. 28

EXECUTIVE SUMMARY

The disposal of low-level radioactiv waste (LLW) in below-ground waste disposal facilities, and the ensuing potential risks of soil and water contamination highlight the need for a comprehensive approach to subsurface hydrologic flow and transport modeling of isotopes at these sites. Numerical and analytical groundwater hydrologic models have been shown to adequately model physical and chemical flow and transport processes, however, the applicability of a model to a particular site becomes questionable if the proper site parameters are not used. This report outlines a systematic approach to parameter estimation, applies this approach to data for a hypothetical (LLW) site to obtain effective hydraulic parameters, uses these parameters in a numerical model, and discusses the uncertainties of the results.

This methodology of parameter estimation is based on stochastic groundwater theory, developed by Gelhar and others, and is used to estimate effective values of hydraulic conductivity, macrodispersivity, and macrodispersivity enhancement. Estimates of macrodispersivity enhancement given by the theory result in significantly higher model concentration predictions over those observed for an unenhanced dispersivity. Since the unenhanced values are typically those used in practice, traditional approaches would tend to severely underestimate concentration levels relative to those predicted considering macrodispersivity enhancement.

Because this parameter derivation is dependent upon the spatial variability of aquifer and isotope characteristics, it is essential to have an accurate quantification of these properties. Variability in the parameter characterization of these properties has a large effect on the effective parameters. Specifically, because of their importance in estimating macrodispersivity enhancement, measurements of isotope sorption should be made on the same soil samples as are measurements of hydraulic conductivity. This will ensure an explicit correlation of these two characteristics.

The magnitudes of the input effective parameters have a severe effect on model results. The sensitivity of the model to these input parameters contributes to uncertainty in the model contamination predictions. This uncertainty is evaluated using a representative analytical model and is found to be significant. It is therefore important to realize that the contamination predictions discussed in this report are only rough order of magnitude estimates.

The numerical model is used to represent saturated contaminant transport from the site to a nearby spring. The importance of the representation of the spatially-varying flow field at the site is emphasized by a comparison of the results of the two-dimensional numerical model for four isotopes with the results of simplified analytical screening calculations. The simplified uniform flow models underestimate the effective spreading of the plume and the level of concentration at low timesrelative to the numerical model. The contamination predictions of the numerical model are compared to drinking water levels for the four input isotopes. For the data used in representing the hypothetical site, most of the isotopes exhibit concentration levels that are close to the drinking water limit. For this reason, it is especially important to understand the uncertainties in the model results.

An additional numerical radial model is created to simulate the potential for long-distance contaminant transport to a hypothetical pumping well. Although this model is only evaluated for a single isotope input, levels of contamination at the well are not found to reach meaningful levels in terms of quantitative evaluation.

Recommendations for future work in this area include an evaluation of the unsaturated zone effects and a three-dimensional model configuration that would incorporate the effects of lateral flux and transverse lateral dispersivity. Additionally, a more extensive approach to evaluating model uncertainties should be developed.

FOREWORD

This technical report was prepared by the Massachusetts Institute of Technology as part of their research project with the Waste Management Branch in the Office of Nuclear Regulatory Research (FIN D2044). This report presents numerical simulation results using a groundwater flow and contaminant transport modeling approach. This work is published as the third volume in a series (NUREG/CR-6114) of contractors' reports which provide auxiliary analyses in support of the NRC staff development and testing of a performance assessment methodology for low-level radioactive waste (LLW) facilities. This document provides technical discussion of issues arising from implementation of MIT's groundwater flow and contaminant transport analysis approach for analyzing a hypothetical LLW facility as defined by the NRC staff

Volume 3 of NUREG/CR-6114 is not a substitute for NRC regulations, and compliance is not required. The approaches and/or methods described in this NUREG/CR are provided for information only. Publication of this report does not necessarily constitute NRC approval or agreement with the information contained herein.

ACKNOWLEDGEMENTS

The research described in this report is part of a continuing study of contaminant transport supported by the U.S. Nuclear Regulatory Commission (USNRC) through the research project entitled, "Improved Methods for Predicting Field-Scale Contaminant Transport" (Contract No. NRC-04-88-074).

The USNRC contributed to the direction and guidance of this work and was responsible for supplying important data and documents. Specifically, Thomas Nicholson coordinated the research efforts of the USNRC, MIT, and the other institutions that contributed to other volumes of this project. He also provided us with the opportunity to meet with the research team at the USNRC in a group meeting, where he raised many topical issues. Also at USNRC, Andrew Campbell and Ralph Cady were very helpful in supplying us with documents and results of their research. Ralph Cady's calculations are the basis for the input concentration values in this report, and Andrew Campbell's work on sorption is relied upon heavily in this document.

Vivek Kapoor, at MIT, was indispensable to the initial stages of the research. His assistance with the model configuration and with the initial theoretical computations was essential for later progress. At Princeton, Michael Celia, an author of another volume in this NUREG series, also contributed many good suggestions for the model configuration.

At Geraghty and Miller, Inc., Greg and Linda Ruskauff provided computer support and software updates.

ABBREVIATIONS

a	intercept
A_0	non-enhanced longitudinal macrodispersivity
A_{11}	enhanced longitudinal macrodispersivity
A_{33}	transverse vertical macrodispersivity
b	aquifer thickness
C	concentration
$\overline{C}$	mean concentration
C_0	input concentration
C_{max}	peak concentration
C_{ss}	steady-state concentration
g_{11}	correlation scale function
g_{33}	correlation scale function
J	mean hydraulic gradient
k	decay coefficient
K_{11}	horizontal hydraulic conductivity
K_{33}	vertical hydraulic conductivity
$\overline{K_d}$	mean sorption coeficient
K_d	linear sorption distribution coefficient
K_{dG}	geometric mean of K_d
K_G	geometric mean of hydraulic conductivity
K_s	saturated hydraulic conductivity
$\ln K$	natural logarithm of hydraulic conductivity
M	isotope inventory
n	porosity
$\overline{pH}$	mean pH
q	specific discharge
Q	pumping rate
Q_s	site pumping rate
Q_{total}	total flux
Q_{trench}	flux through trenches
$\overline{R}$	effective retardation
R	retardation factor
s	well drawdown
$\hat{t}$	dummy variable
t	time
t_p	peak time
t_{unsat}	unsaturated travel time
$\hat{v}$	retarded velocity
v	water velocity
v_{sat}	saturated water velocity
v_{unsat}	unsaturated water velocity
w	site width
$\hat{x}$	dummy variable
x	horizontal distance
z	vertical distance
$\overline{\%clay}$	mean clay content
α	angle
β	coefficient in pulse solution
χ	rate constant
ε	recharge
ϕ	drawdown
γ	flow factor
η	residual
κ	spatial decay rate
λ_1	horizontal correlation scale
λ_3	vertical correlation scale
λ_η	correlation scale for residual
π	pi
Θ	moisture content
θ	angle
ρ_b	bulk density
$\sigma_{\%clay}$	standard deviation of $\%clay$
σ_C	standard deviation of concentration
σ_{Kd}	standard deviation of K_d
$\sigma_{\ln K}$	standard deviation of $\ln K$
$\sigma_{\ln Kd}$	standard deviation of $\ln K_d$
σ_{pH}	standard deviation of pH
σ_R	standard deviation of retardation
ζ	correlation factor

CHAPTER 1
INTRODUCTION

As progress is made in the fields of nuclear power, medicine, cell biology, and other areas of scientific research, an increasing amount of low-level nuclear waste is generated. Disposal of this waste is a concern throughout the United States. Agreement States have the responsibility for licensing low-level radioactive waste (LLW) disposal facilities. The United States Nuclear Regulatory Commission (USNRC) provides assistance to the Agreement States in the form of Federal Regulations and guidance for licensing LLW facilities. At a LLW site, the potential for radioactive contamination of the air, water, and soil needs to be assessed through performance assessments. The licensee has the responsibility for conducting performance assessments and monitoring the LLW facilities. These assessments include hydrologic models appropriate to the various sites. Because LLW facilities typically dispose of waste below ground, groundwater models are important parts of the overall assessment. This report presents a methodology for the systematic determination of hydraulic input parameters to a groundwater model of a hypothetical LLW facility. This methodology is designed to be appropriate to LLW facility performance assessments.

Analysis of subsurface contaminant transport is considerably more complex than it is for surface water bodies. The high degree of natural spatial heterogeneity in soils, the difficulty in obtaining measurements of large-scale behavior, and the long time scales over which this behavior occurs all contribute to a complication of the analysis (Polmann *et al.*, 1988, p. 1-1). Additionally, a true discrete description of the subsurface conditions is infeasible, both because of cost limitations in data gathering, and because the drilling of numerous wells for gathering adequate data would itself affect the hydraulic properties of the aquifer. For these reasons, a statistical or stochastic approach to the quantification of hydraulic properties seems ideally suited for subsurface conditions. Data collected from several locations may be collectively analyzed to determine the mean and variance of the data set. These statistical quantities describe the characteristics of the measured hydraulic property at every location. This stochastic theory is well-developed in the field of subsurface hydrology and is described in detail in Gelhar (1993).

The most difficult aspect of groundwater modeling is the determination of appropriate hydraulic input parameters. Traditionally, a rough estimate or an average of a few measurements is often the basis for the selection of a particular parameter value. As is shown in this report, however, commonly available site data sources can be combined with the application of stochastic theory to result in a more systematic approach to hydraulic parameter estimation.

In order to demonstrate this process, a hypothetical LLW facility is created. Situated in a coastal plain environment in a humid climate, the hypothetical facility is used as an example for conducting and testing performance assessment modeling. Data on measured soil properties, typical of the types of measurements available at other sites, are assigned to the hypothetical site for the purposes of illustrating the analysis. These data are analyzed using the saturated stochastic flow and transport theory presented in Gelhar and Axness (1983).

The application of the theory to the site data results in estimates for several effective hydraulic parameters, including hydraulic conductivity, macrodispersivity, and macrodispersivity enhancement. These parameters are used as inputs to a two-dimensional numerical flow and transport computer code. This simulation is typical of the types of models commonly employed in the evaluation of groundwater flow and transport problems. The use of the numerical model shows how the stochastic parameter estimation may be combined with a traditional numerical modeling approach.

In this report, several illustrative input examples are modeled using various isotope contaminants and model configurations. The sensitivity of the numerical model to variations in input parameters is explored. Additionally, the numerical model concentration predictions are compared to those of simplified analytical screening calculations to show the importance of accurately representing the spatially-varying flow field at the site. It is emphasized that results of the parameter estimation and modeling processes are subject to uncertainties. These uncertainties result from sensitivities of the mean concentration solutions to input parameters and from stochastic variation around the mean solution. Although these uncertainties are evaluated to an extent in this report, future work should include a more rigorous analysis of some of the other causes of uncertainty. Some of these include unsaturated flow effects, a larger model extent, and an inclusion of different isotope inputs.

A major conclusion of this report is that the magnitudes of the hydraulic input parameters have a severe effect on the model results. This observation underscores the need for a systematic approach to hydraulic parameter estimation, and for a diligence in obtaining relevant site data measurements that compliment the parameter estimation process.

CHAPTER 2
SITE CHARACTERISTICS

As stated in the introduction, the purpose of this report is to apply modeling techniques to a hypothetical low-level radioactive waste (LLW) disposal facility. Some hypothetical characteristics of the site and its hydrology and geology are defined in this chapter as background for the later discussion of the analysis. This hypothetical site was created for use in this report, and will subsequently be referred to in the present tense.

2.1 General Description

The hypothetical site is approximately one kilometer square in size and is located in a humid climate. Average annual precipitation is about 1.2 meters per year and is distributed evenly throughout the year. Sixty to seventy percent of the precipitation is lost to evapotranspiration, yielding a net recharge to the groundwater system of 0.40 meters per year. As a LLW facility, the site receives about 75 percent of its waste from non-fuel aspects of the nuclear power industry, with the remaining 25 percent from industrial, medical, and academic sources. The waste is buried in standard 210-liter Department of Transportation steel drums that are placed in trenches and covered with sand and a clay cap. These burial trenches are 15-30 meters wide, 150-300 meters long, and 7 meters deep. On average, there are 50 trenches at the site, spaced 3 meters apart. The minimum distance between the bottom of the trenches and the water table is 1.2 meters.

2.2 Site Geology and Hydrology

The geology of the site is that of coastal plain sediments. It is characterized by thick, expansive horizontal layers of sediments with lateral extents of hundreds of kilometers. Sediments are relatively homogeneous within layers and consist primarily of sands, silts, and some clay lenses and confining beds. Three identifiable hydrologic zones make up the water table aquifer. These zones are 10-50 meters thick and exhibit distinct hydrologic properties. A confining bed of clay that is 20 meters thick forms the horizontal base of the phreatic aquifer at a depth of around 100 meters. The three zones are labeled Zone 1, Zone 2, and Zone 3, in order of increasing depth. In general, permeability increases with depth, such that Zone 3 is more permeable than Zone 2, and Zone 2 is more permeable than Zone 1 (Cahill, 1982).

At this humid site, the water table is close to the ground surface. The unsaturated zone is relatively thin, extending only 8-14 meters below the surface. Because the trench depth places the waste 1-2 meters above the water table, it is expected that the unsaturated zone plays a minimal role in the overall travel of the contaminants through the groundwater system. This is discussed in greater detail in Chapter 3.

The mean horizontal gradient is fairly uniform across the site. Therefore, flow at any point in the site would be expected to be roughly in the same direction. The mean horizontal gradient is taken to be 0.01, in the direction of a nearby spring (Cahill, 1982), as shown in Figure 2-1.

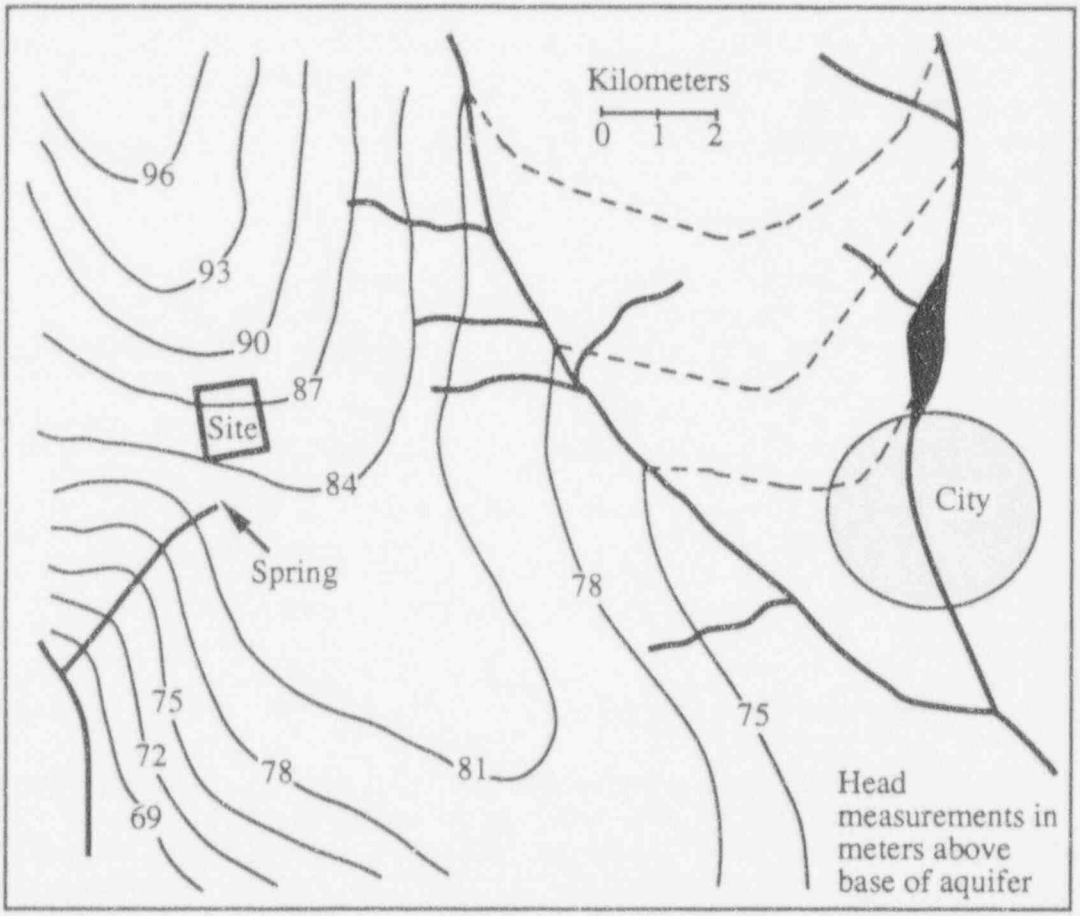

Figure 2-1 Map of hypothetical LLW site showing water table contours, relative scale, and proximity to spring and city.

CHAPTER 3
PARAMETER ESTIMATION

Hydraulic parameters can be estimated through the application of stochastic theory to groundwater characteristics of the site, gathered from traditional data sources. This chapter describes the data sources, outlines the theory, and provides a step-by-step methodology of the parameter estimation process as applied to representative site data.

3.1 Sources of Data

The data used in this hypothetical model are drawn from several available sources. The sources used are representative of those available for other, actual sites. Specifically, the quantitative information provided by Cahill (1982) serves as representative data for the hypothetical site. This section provides a description of the sources and a compilation of the data that are used in deriving the traditional input parameters for a discrete numerical groundwater flow and transport model.

Precipitation and recharge measurements from the U.S. National Weather Service at specific locations are averaged over the last 50 years to obtain estimates of the flow input to a model. Hydraulic gradients, water table shape, and head distributions are calculated on the basis of recorded water levels from on-site and local wells.

Data on hydraulic conductivity, K, are compiled from several different sources. As taken from Cahill (1982), they comprise a collection of values obtained from laboratory tests on core samples and measurements from in-situ aquifer testing. Specifically, results of hydraulic conductivity tests on core samples taken at various depths from seven different wells are combined with measurements of K from on-site slug tests, an aquifer test in the upper 60 meters of sediments, and the specific capacity of a local pumping well, as shown in Figure 3-1. This compilation of a hydraulic conductivity data set is analyzed using stochastic theory, as described in Section 3.2.

Data on pH are compiled from water samples at site wells (Cahill, 1982), and from measurements in similar settings at a nearby site (Goode, 1986). The variation of pH is an important parameter when modeling contaminant transport, as discussed in Chapter 4.

3.2 Saturated Zone

Stochastic parameter estimation in the saturated zone involves the application of stochastic theory, as developed by Gelhar and Axness (1983), to a set of site data for the purposes of yielding effective parameters. The site data are statistically evaluated to obtain values of the mean and standard deviation. These values are then used in equations furnished by the theory to give effective parameters. These parameters incorporate the mean and variation characteristics of the original data. The effective parameters are then used in a traditional discrete numerical model, as outlined in Chapter 5. The following sections describe the application of stochastic theory to

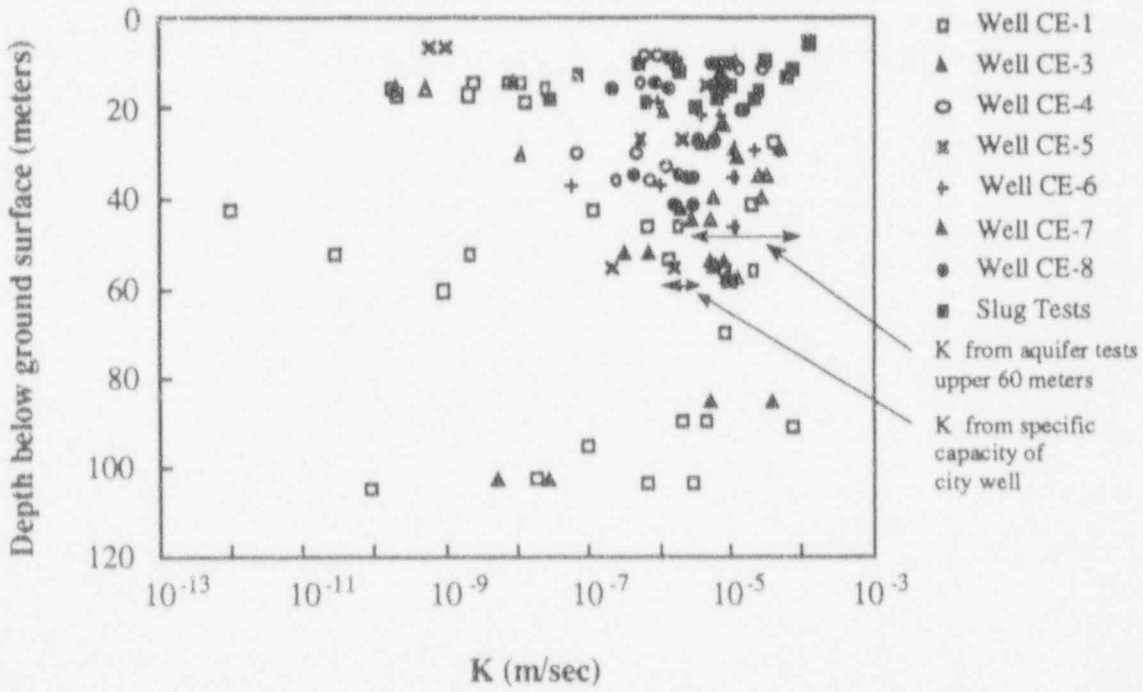

Figure 3-1 Collected values of hydraulic conductivity versus depth. From laboratory tests on soil samples from seven wells, on-site slug tests, an aquifer test, and specific capacity of a local city well; data compiled from Cahill (1982).

parameter estimation of hydraulic conductivity, macrodispersivity, and macrodispersivity enhancement for sorbing species.

3.2.1 Correlation Scales

For heterogeneous soils, the correlation scale is defined as the distance from a hydraulic conductivity measurement beyond which it is expected that a second hydraulic conductivity measurement will be unrelated. Within a single correlation distance, measurements are related or dependent. In sedimentary systems, the vertical and horizontal correlation scales are usually very different, with the horizontal (parallel to bedding) correlation scale orders of magnitude larger than the vertical correlation scale.

Approximating the correlation scales is usually the most difficult process in parameter estimation. In the coastal plain sediments of this hypothetical site, clay lenses are common features. A measurement of the average vertical thickness of the clay lenses serves as a proxy for the correlation scale in the vertical direction, λ_3, since two measurements in the vertical direction that are further apart than this thickness will not encounter the same lens. On the site, clay lens thicknesses are observed and recorded in well-drillers' logs. A compilation of these measurements is given in the histogram in Figure 3-2. An evaluation of the distribution of clay lens thicknesses in Figure 3-2 produces an average thickness of approximately 1 meter. On the basis of this observation, the vertical correlation scale is taken to be 1 meter.

Gelhar (1993) has shown that, for many different sites, the horizontal correlation scale is related to the overall problem scale. In Figure 3-3, Gelhar (1993) demonstrates a one-to one relationship between the log of the horizontal correlation scale and the log of the overall scale, such that the correlation scale is on average one order of magnitude smaller than the overall scale. For the hypothetical site in this report, the downgradient distance from the site to the spring is the primary path of concern (see the map in Figure 2-1). This distance is approximately 1300 meters, and it defines the overall problem scale for the two-dimensional rectangular model discussed in Chapter 5. From Figure 3-3, for an overall problem scale of 1000 meters, there is a corresponding horizontal correlation scale, λ_1, of 100 meters. Therefore, for this site, using a model on the order of 1000 meters in length, the correlation scales are $\lambda_3 = 1$ meter, $\lambda_1 = 100$ meters, and $\lambda_1/\lambda_3 = 100$. Because little information is available that would indicate a difference in correlation scales for the three hydraulic zones, the same values for the correlation scales are used in all three zones.

3.2.2 Hydraulic Conductivity

The principal components of hydraulic conductivity for the three dimensional (3D) anisotropic system at the site with isotropy in the plane of bedding ($\lambda_1 = \lambda_2 >> \lambda_3$) may be defined in the horizontal direction, K_{11}, and in the vertical direction, K_{33}. Using theory outlined in Gelhar and Axness (1983), in a system with mean flow parallel to bedding, expressions of K_{11} and K_{33} may be written as a function of the correlation scales and of the statistics of the hydraulic conductivity data.

$$K_{11} = K_G \exp\left[\sigma^2_{\ln K}\,(0.5 - g_{11})\right]; \quad g_{11} = f_1(\lambda_1 / \lambda_3) \tag{3.1}$$

$$K_{33} = K_G \exp\left[\sigma^2_{\ln K}\,(0.5 - g_{33})\right]; \quad g_{33} = f_3(\lambda_1 / \lambda_3) \tag{3.2}$$

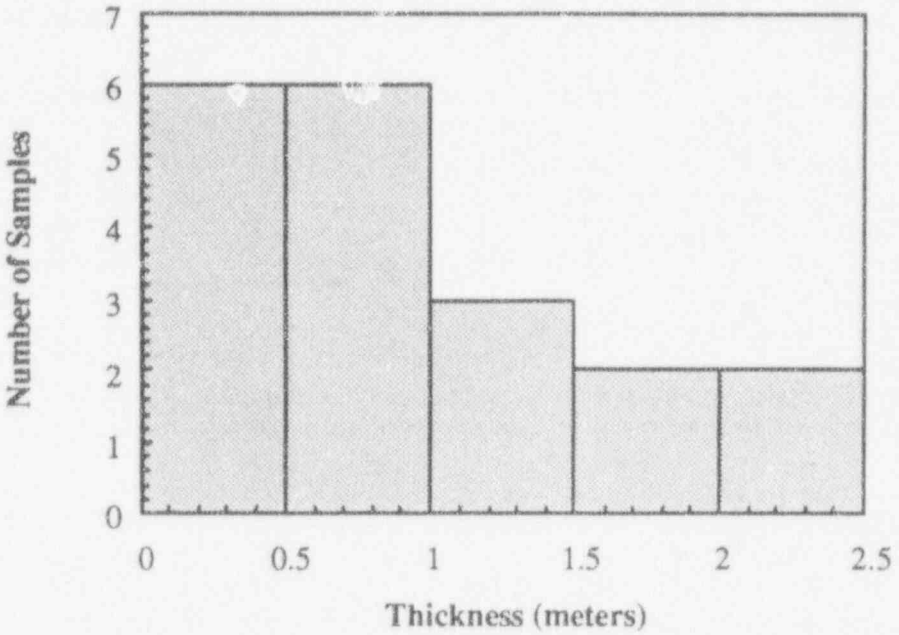

Figure 3-2 Histogram showing distribution of thickness of clay lenses for nineteen observations from well-drilling logs; observations from unpublished well-drillers' logs.

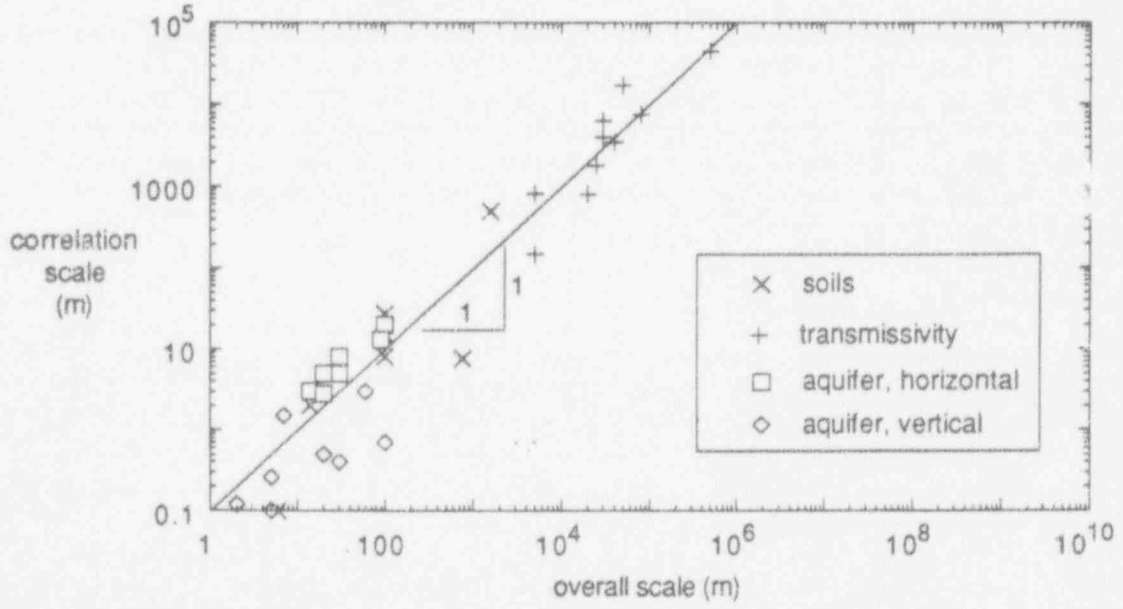

Figure 3-3 Horizontal correlation scale of hydraulic conductivity, λ_1, as compared to overall problem scale, reproduced from Gelhar (1993, Figure 6.5b, page 292).

where K_G is the geometric mean of the hydraulic conductivity data set such that $\ln K_G = E[\ln K]$, with $\ln K$ indicating the natural logarithm of K. $\sigma^2_{\ln K}$ is the variance of $\ln K$, and g_{11} and g_{33} are functions of λ_1/λ_3 given by Gelhar and Axness (1983, p. 167). These functions have values less than one, with $g_{11} << g_{33}$ when $\lambda_1 >> \lambda_3$. This description assumes a lognormal distribution of K, as is commonly seen in field examples.

The parameters K_G and $\sigma^2_{\ln K}$ for each zone are estimated through a statistical analysis of the values of K in that zone, based on the data in Figure 3-1. It is found, however, that while calculated values of K_G appear to be of a reasonable magnitude, calculated values of $\sigma^2_{\ln K}$ for the hypothetical site data set are noticeably larger than those expected on the basis of comparison with other sites. All three zones exhibit this behavior, with Zone 1 having the largest value of $\sigma^2_{\ln K}$, and Zone 3 the smallest value. The extremely large values of $\sigma^2_{\ln K}$ reflect the strong influence of a small number of very low conductivity values shown in Figure 3-1. Such low values are expected to have a minimal effect on transport because the water is practically immobile in regions with conductivities several orders of magnitude below the geometric mean. Gelhar (1993) presents a comparison of the standard deviation of $\ln K$, $\sigma_{\ln K}$, with overall problem scale, as shown in Figure 3-4. This figure represents a compilation of data from many sites, and indicates that values of $\sigma_{\ln K} \leq 2.5$ would be reasonable estimates. Maintaining the same relative magnitudes of $\sigma_{\ln K}$ for the three zones, estimates of $\sigma_{\ln K}$ are selected on the basis of the relationship in Figure 3-4. These values are displayed with the data in Figure 3-5.

The computed values of K_G, and the selected values of $\sigma_{\ln K}$ are input into Equations 3.1 and 3.2 to give results for K_{11} and K_{33}. This analysis is performed for each zone and for the aquifer evaluated as a whole (disregarding the various zones). These values of K_{11} and K_{33} are then entered into the 2D rectangular finite-element model described in Chapter 5, and adjusted upward slightly in the calibration of the model with recharge. A comparison of K_{11} and K_{33} with the entire data set appears in Figure 3-6. A summary of the final parameters is shown in Table 3-1.

3.2.3 Macrodispersivity

While correlation scales and hydraulic conductivity parameter estimation are sufficient as a description of a flow system, for modeling transport it is necessary to describe the spreading of the contaminant plume as well. A description of the spreading in the direction of flow is given by the longitudinal macrodispersivity, A_0, and in the vertical direction perpendicular to the flow by the transverse vertical macrodispersivity, A_{33}. The theory supplied by Gelhar and Axness (1983) provides an expression for longitudinal macrodispersivity:

$$A_0 = \frac{\sigma^2_{\ln K} \lambda_1}{\gamma^2} \tag{3.3}$$

where $\sigma^2_{\ln K}$ is the variance of $\ln K$, and λ_1 is the horizontal correlation scale. The flow factor, γ, is defined by the following:

$$\gamma = \frac{q}{K_G J} \tag{3.4}$$

where q is the specific discharge and J is the mean hydraulic gradient. Gelhar and Axness (1983) show that γ may be expressed as a function of $\sigma^2_{\ln K}$, g_{11}, g_{33}, and the angle, θ, between the mean flow direction and the bedding plane, as given in the following:

Table 3-1 Summary of hydraulic parameters

	average saturated thickness (m)	$\sigma^2_{\ln K}$	K_G (m/s)	K_{11} (m/s)	K_{33} (m/s)	K_{11}/K_{33}	λ_1 (m)	λ_3 (m)
Zone 1	8	4.4	8.5E-07	7.5E-06	1.0E-07	74	100	1
Zone 2	24	3.6	2.5E-06	1.5E-05	4.4E-07	34	100	1
Zone 3	48	3.2	6.1E-06	3.0E-05	1.3E-06	23	100	1
total aquifer	80	4.0	2.6E-06	1.9E-05	3.8E-07	50	100	1

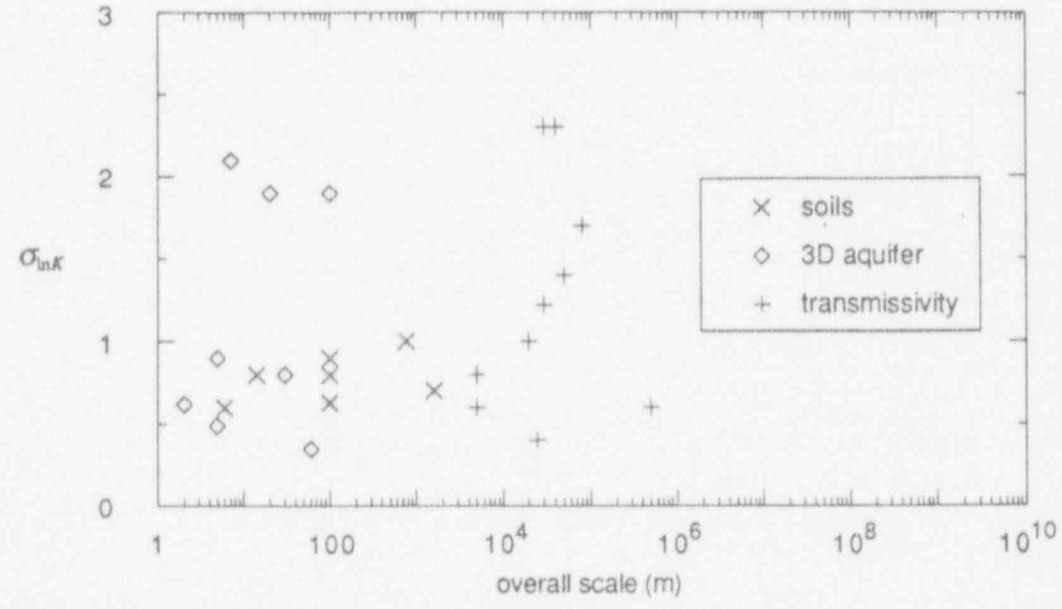

Figure 3-4 Standard deviation of hydraulic conductivity, $\sigma_{\ln K}$, as compared to overall problem scale for a collection of site examples; reproduced from Gelhar (1993, figure 6.5a, p. 292)

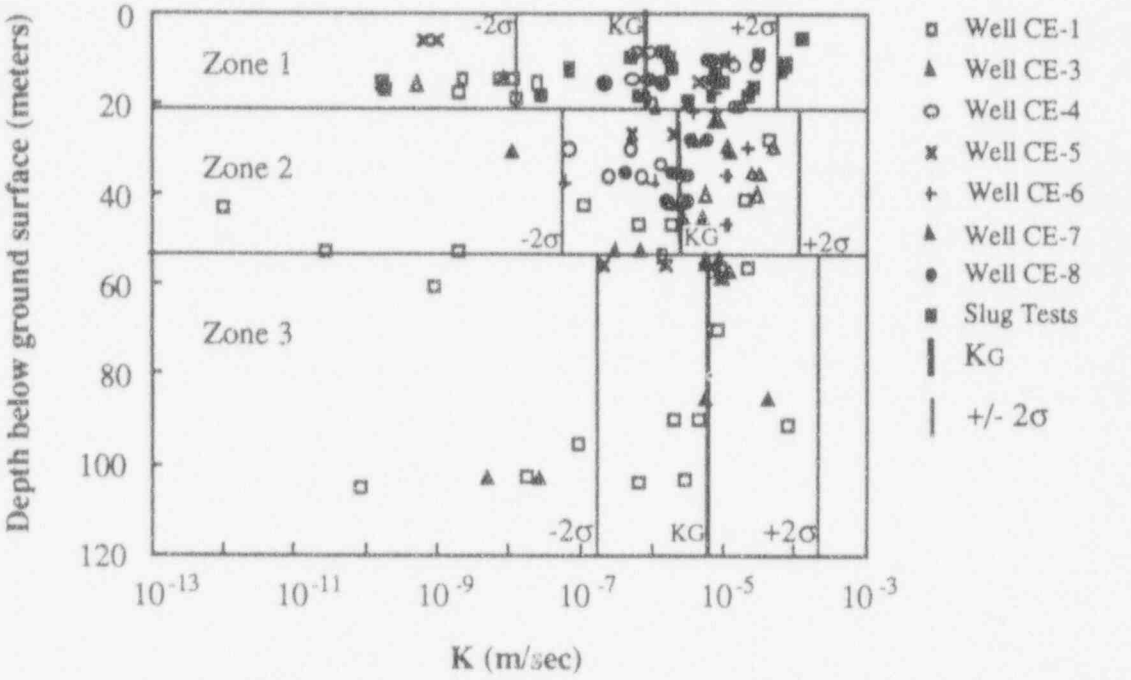

Figure 3-5 Graph showing relationship of K_G and $\sigma_{\ln K}$ for each zone to compilation of hydraulic conductivity data from Figure 3-1.

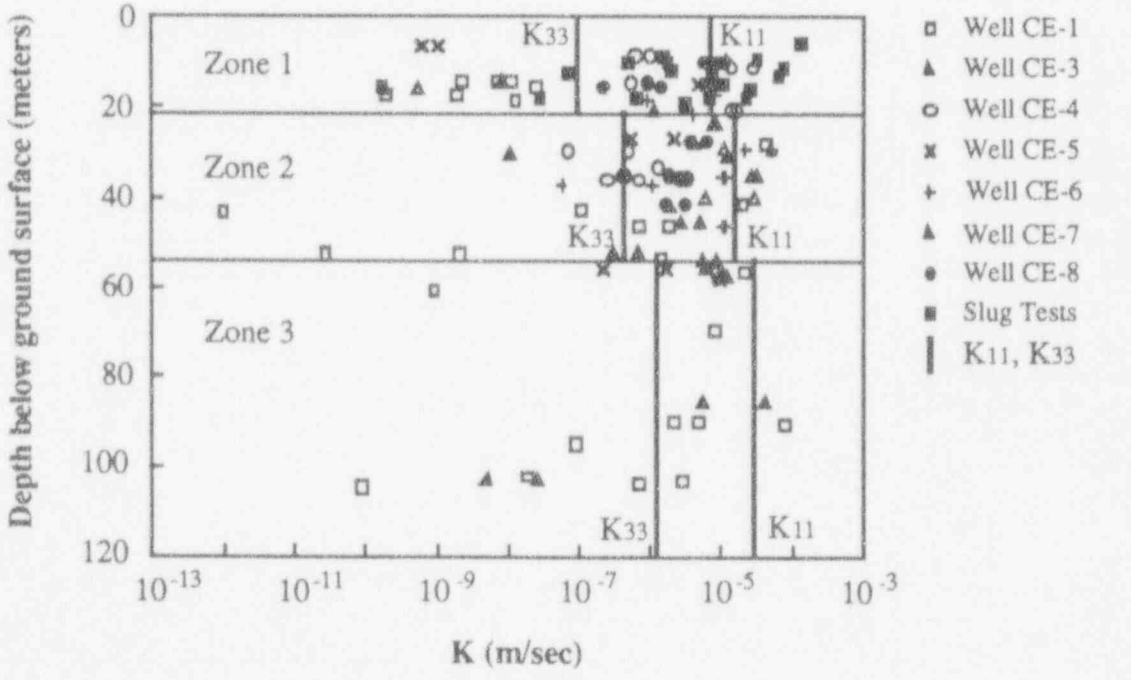

Figure 3-6 Graph showing relationship of K_{11} and K_{33} for each zone to compilation of hydraulic conductivity data from Figure 3-1.

$$\gamma = \frac{\exp\left[\sigma^2_{\ln K}(0.5 - g_{33})\right]}{\sin^2\theta + \left\{\exp\left[\sigma^2_{\ln K}(g_{11} - g_{33})\right]\right\}\cos^2\theta} \tag{3.5}$$

For the particular attributes selected for the hypothetical LLW site, water will flow vertically under the site when it enters as recharge beneath the trenches, and when it discharges to the spring. At those locations, θ will be 90 degrees from the horizontal bedding. However, for the most part, along the 1300 meter distance between the site and the spring, the flow is horizontal (parallel to the bedding), and θ is zero. Ideally, θ would be calculated at every point in the flow path and used to describe a spatially-varying longitudinal macrodispersivity at different points in the flow field. In practice, however, computer codes, such as the SUTRA code used here, are not configured to make these calculations, and a mean θ is used to compute a mean γ and, subsequently, a mean A_0.

A mean value of $\theta = 7$ degrees is selected to incorporate the influence of the overriding horizontal flow. This value of θ corresponds to $\gamma = 4$, and produces a longitudinal macrodispersivity of $A_0 = 25$ meters. This value is in the range of measurements of A_0 collected from other sites, as shown in the graph in Figure 3-7, reproduced from Gelhar *et al.*, (1992, figure 2).

For a 3D model with flow parallel to the bedding, transverse vertical macrodispersivity, A_{33}, is expected to be very small. It is known that unsteady flow effects can have a strong influence on transverse macrodispersion (Rehfeldt and Gelhar, 1992). There is no explicit information on temporal fluctuations in hydraulic gradient at this site so that, based on the experimental results summarized in Gelhar *et al.* (1992, figure 4), it is assumed that $A_0/A_{33} \approx 100$, and that $A_{33} = 0.25$ meters.

3.2.4 Longitudinal Macrodispersivity Enhancement through Sorption Variability

Another parameter of importance in modeling contaminant transport is the distribution coefficient, K_d, which characterizes reversible, linear sorption. This contaminant-dependent and soil-dependent quantity describes the partitioning of the contaminant between the soil and the water. The net effect of sorption is to retard the velocity of the contaminant in the soil. Because sorption for specific contaminants may be a function of soil properties, as the soil properties experience spatial variation, the sorption also varies. This variation directly affects the velocity of the contaminant, which, in turn, enhances the spreading of the plume. The enhanced spreading is defined by a larger reactive longitudinal macrodispersivity, A_{11}, as distinguished from A_0, the non-reactive longitudinal macrodispersivity. The increased plume spreading, over that which would be the result for no sorption, is defined as the macrodispersivity enhancement, A_{11}/A_0. It is important to note that the theory indicates this effect of macrodispersivity enhancement only occurs in the longitudinal direction. The transverse macrodispersivity is unaffected by sorption variability, as discussed in Garabedian *et al.* (1988).

In order to understand clearly the importance of spatially variable sorption, a number of parameters must be defined. The variable K_d may be described by a mean ($\overline{K}_d$) and a standard deviation (σ_{Kd}). Further, the retardation factor, R, is related to K_d by the following:

$$R = 1 + \frac{\rho_b K_d}{n} \tag{3.6}$$

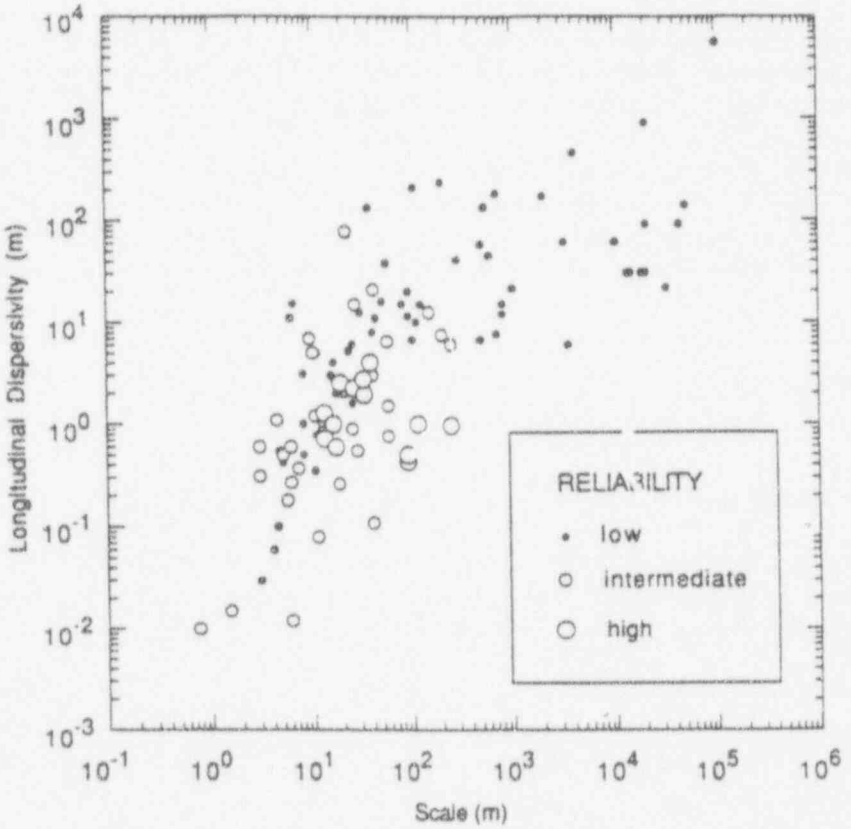

Figure 3-7 Longitudinal macrodispersivity versus overall problem scale with data classified by reliability; reproduced from Gelhar *et al.* (1992, figure 2).

where ρ_b is the bulk density (= mass of solid/bulk volume), and n is the soil porosity. R may be described statistically by an effective retardation, $\overline{R} = E[R]$, and by a standard deviation:

$$\sigma_R = \frac{\rho_b}{n}\sigma_{K_d} \tag{3.7}$$

By analyzing the mean and variation of a sample data set of a measured soil property, and by showing a relationship between the soil property and R, $\overline{R}$ and σ_R may be calculated as a function of the statistics of the soil property data set.

In addition, R may be related to $\ln K$ as shown in Figure 3-8. In Figure 3-8, ζ is the fraction of $\sigma_R^2 / \overline{R}^2$ that is correlated with $\ln K$, and η is the residual. η is taken to be a zero mean stochastic process that is uncorrelated with $\ln K$. When $\zeta = 1$, there is perfect correlation, and $\eta = 0$. When $\zeta = 0$, the variables are uncorrelated. As given by the relationship in Figure 3-8:

$$R = a - \left(\frac{\sigma_R}{\sigma_{\ln K}}\sqrt{\zeta}\right)\ln K + \eta \tag{3.8}$$

where a is the intercept.

The net result of the variation in the retardation and the relationship between retardation and $\ln K$ is to increase the longitudinal macrodispersivity of the sorbed species according to the following equation given by Gelhar (1993, p. 256):

$$A_{11} = A_0\left\{\left[1 + \gamma\frac{\sigma_R}{\overline{R}\,\sigma_{\ln K}}\sqrt{\zeta}\right]^2 + (1-\zeta)\frac{\sigma_R^2\,\lambda_\eta}{\overline{R}^2\,\sigma_{\ln K}^2\,\lambda_1}\gamma^2\right\} \tag{3.9}$$

where A_0 is the non-reactive longitudinal macrodispersivity, λ_1 is the horizontal correlation scale, $\lambda_\eta \approx \lambda_1$, and γ is as defined in Subsection 3.2.3. The result of the longitudinal macrodispersivity enhancement is to extend significantly the leading edge of the plume. The effect of enhancement on transport becomes particularly important for contaminants that exhibit a first order decay and possess a half-life that is on the same order of magnitude as the peak travel time (see Chapter 4). As will be seen in Chapter 5, in this case the enhanced macrodispersivity results in much larger concentrations at early time.

3.3 Unsaturated Zone

The characteristics selected for the hypothetical LLW site result in an unsaturated zone thickness that is small in comparison to the saturated thickness. To determine if the unsaturated zone may be neglected in a 2D vertical cross-sectional site model, some rough calculations are performed. If the expected travel time in the unsaturated zone is much shorter than the expected saturated travel time from the site to the spring, then it is assumed to be reasonable to neglect the unsaturated zone in the model.

Using a saturated vertical hydraulic conductivity, K_s = 1.0 E-7 m/s (see Table 3-1); an average moisture content, $\Theta = 0.28$ (Dennehy and McMahon, 1987); and a

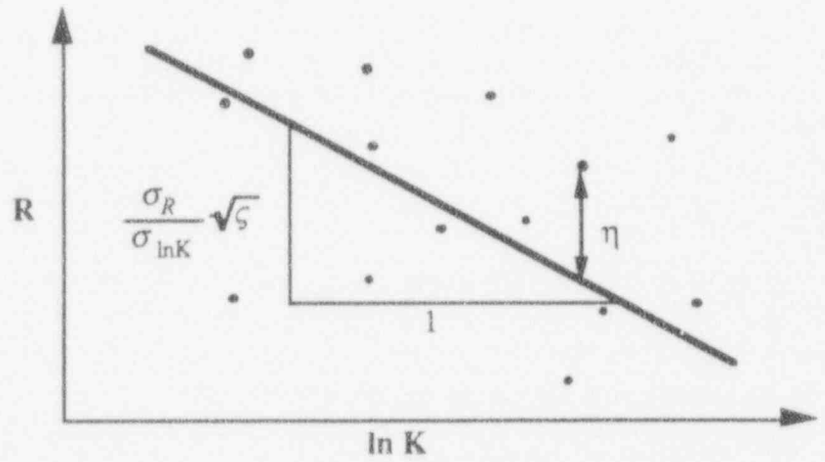

Figure 3-8 Relationship between R and $\ln K$ showing correlation factor, ζ, and residual, η.

steady recharge, $\varepsilon = 0.4$ m/year, the vertical velocity of the water in the unsaturated zone is given by:

$$v_{unsat} = \frac{\varepsilon}{\theta} = 1.4 \text{ m/yr} \tag{3.10}$$

The value of recharge represents a worst-case scenario, assuming that all the recharge that enters the soil will enter the trenches and will subsequently percolate through the bottom of the trenches to the water table. For a distance from the bottom of the trench to the water table, $z = 1.5$ meters (see Figure 3-9), the unsaturated travel time is then:

$$t_{unsat} = \frac{z}{v_{unsat}} = 1.1 \text{ years} \tag{3.11}$$

Even considering longitudinal dispersivity in the unsaturated zone, the travel time is still on the order of 10^0 years, a relatively short time for a hydrological system.

In the saturated zone, using a porosity, $n = 0.4$; a mean hydraulic gradient, $J = 0.011$; a horizontal hydraulic conductivity of the total aquifer, $K_{11} = 1.9$ E-5 m/s (see Table 3-1); and assuming predominantly horizontal flow, the velocity in the saturated zone is calculated as:

$$v_{sat} = \frac{K_{11} J}{n} = 17.3 \text{ m/yr} \tag{3.12}$$

For a horizontal distance from the site to the spring, $x = 1300$ meters, the saturated travel time is given by

$$t_{sat} = \frac{x}{v_{sat}} = 75 \text{ years} \tag{3.13}$$

On the basis of these calculations, since $t_{unsat} << t_{sat}$, for the particular site configuration of this hypothetical LLW problem, the unsaturated zone flow and transport is neglected from further analysis. Neglecting the unsaturated zone is not a good assumption for all sites, however. At other humid sites there may be other considerations, such as unsteady recharge or volatile contaminants, where the unsaturated zone plays a more important role. Likewise, at arid sites where the unsaturated zone is very thick, modeling the unsaturated zone is essential to the problem.

If the unsaturated zone is to be modeled for a particular site, the effective unsaturated hydraulic conductivity and moisture retention curve may be derived using stochastic theory much in the same way as are the saturated parameters. Although this theory is not expanded upon in depth in this paper, other authors devote their attention to this subject in great detail. Yeh *et al.* (1985) outline this theory for steady flow and present a derivation based on first principles. In two related papers, Mantoglou and Gelhar (1987a, 1987b) explore the application of the theory to parameter estimation of hydraulic conductivity and moisture content for transient unsaturated flow in stratified soils. Polmann (1990) extends the analysis to soil with more complicated and realistic hydraulic characteristic curves, including solute transport as well as flow for large-scale systems. Polmann *et al.* (1988, 1991) use the results of the stochastic analysis in transient numerical simulations. Additionally, Gelhar (1993) presents a comprehensive synopsis of the theory, including several examples of its application.

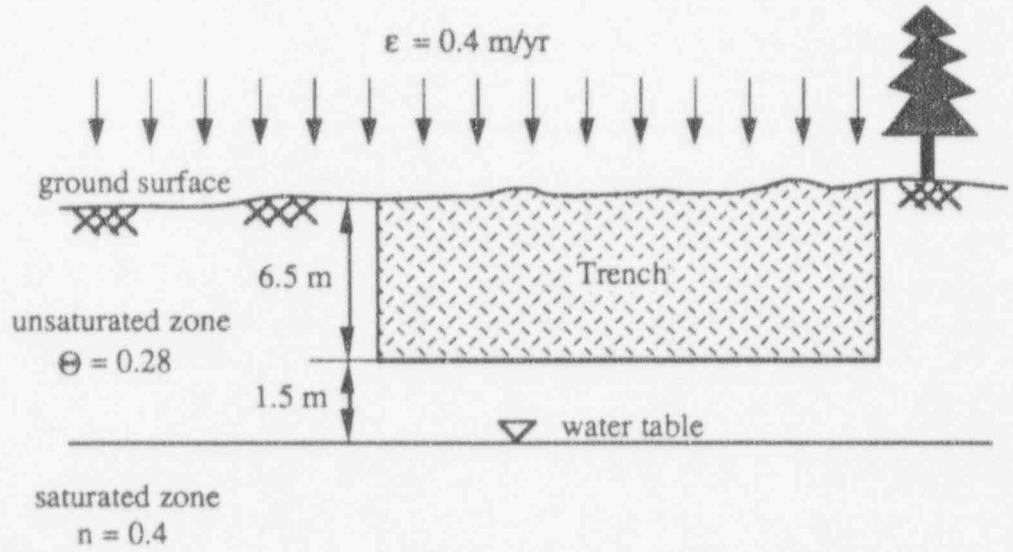

Figure 3-9 Idealized representation of the unsaturated zone in cross-section at the hypothetical site, showing distance from bottom of trench to water table.

CHAPTER 4
ISOTOPE CHARACTERISTICS

Low-level nuclear waste is a combination of waste from many sources and therefore contains many different radionuclides, all of which are potentially a source of contamination. This report provides examples of some transport phenomena, but does not attempt to cover all scenarios. Four isotopes with a variety of characteristics are selected, using a screening process, from a subset of those that potentially compose the waste. The sorption dependence of these isotopes on aquifer characteristics, and the corresponding longitudinal macrodispersivity enhancement is evaluated for use in the 2D numerical model in Chapter 5.

4.1 Screening Process

Isotopes are categorized by solubility and trench inventory as one of two types and are evaluated using two separate screening models. The first screening model is a step input for isotopes that have high trench inventory in comparison to their solubility. The second screening model is a pulse input for isotopes that have high solubility in comparison to their trench inventory. Two isotopes are selected for evaluation using the step input screening model, and two are selected using the pulse input screening model.

Of the isotopes that are typically found in low-level waste, eight are identified as isotopes of interest for modeling at the hypothetical site (see Table 4.1). Assumptions are made regarding the isotope total inventories, expressed in Curies (Ci), and solubilities, expressed in Curies per cubic meter (Ci/m^3) (Campbell, 1992), as displayed in Table 4.1. The time over which an isotope would be completely released from the waste trenches may be defined as the input duration. This definition assumes that a steady recharge rate of water is received by the trenches, and that the solubility of the isotope completely controls the amount of isotope dissolution in the water. The recharge is assumed to be equal to the total recharge received by the site of 0.4 m/year, as defined in Section 2.1. This representation is a worst-case scenario of complete trench failure where the waste is easily available for dissolution in and percolation downward with the water. The input duration is calculated as follows:

$$\textit{Input duration}\,(\text{years}) = \frac{\textit{inventory}\,(\text{Ci})}{\textit{trench area}\,(\text{m}^2) \times \textit{recharge}\,(\text{m/yr}) \times \textit{solubility}\,(\text{Ci/m}^3)} \quad (4.1)$$

where units are displayed in parentheses, and trench area is the plan area of the trenches that contain the isotope. Input durations for the eight isotopes are calculated using Equation 4.1 and are presented in Table 4.1.

As shown in Table 4.1, for all isotopes other than tritium (H-3) and uranium (U-238), the input duration is much smaller than one year. From the perspective of the time scale of a saturated transport problem (see Section 3.3) these isotopes may be treated as having an instantaneous pulse release. That is, as soon as the trenches are breached, immediately all the isotope contamination will be transported by the water. For tritium

Table 4.1 Isotopes of potential interest in modeling.
Inventory and solubility estimates from Campbell (1992).

Isotopes	Inventory (Ci)	Solubility (Ci/m^3)	Input duration (years)	screening type
Am-241	4.46E+00	8.28E+04	1.76E-07	pulse
Co-60	5.34E+05	6.79E+05	2.57E-03	pulse
Cs-137	4.09E+05	1.44E+04	9.20E-02	pulse
H-3	7.65E+06	3.88E+01	6.43E+02	step
I-129	1.86E+00	2.24E-01	2.00E-02	pulse
Sr-90	3.33E+05	1.38E+08	7.85E-06	pulse
Tc-99	1.11E+02	1.94E+03	1.87E-04	pulse
U-238	1.04E+02	2.56E-07	5.46E+04	step

and uranium-238, however, the input duration is much greater than the expected saturated transport time scale. From the perspective of this time scale, tritium and uranium-238 may be modeled as step inputs with large inventories. At the time the trenches are breached, a steady rate of isotope contamination will begin to be transported by the water. This rate will continue throughout the duration of the simulation, eventually reaching a steady state concentration level at every point in the aquifer. All the simulations in this report assume that the trenches and trench covers are breached and that water is free to percolate through the waste to the water table.

4.1.1 Step Input

The step input screening model uses an analytical solution to the 1D transport equation to approximate the steady state concentration (C_{ss}) at some distance (x) from the point of concentration input. A complete derivation of this solution is given in Appendix A. The 1D analytic solution is of the form

$$C_{ss}(x) = C_0 \, e^{-\kappa x} \tag{4.2}$$

where C_0 is the input concentration and κ is a spatial decay rate, which is a function of the decay coefficient (k), the enhanced dispersivity (A_{11}), and the retarded velocity ($\hat{v}$) (see Appendix A). The retarded velocity is a measure of the velocity of the contaminant as compared to v, the velocity of the water:

$$\hat{v} \equiv \frac{v}{R} \tag{4.3}$$

where R is the isotope retardation factor (see Subsection 3.2.4). A related variable, the contaminant travel time, is defined as the distance traveled divided by the retarded velocity. The magnitude of the input concentration, represented as an average over the gross area, is given by

$$C_0 \ (\mathrm{Ci/m^3}) = \frac{solubility \ (\mathrm{Ci/m^3}) \times Q_{trench} \ (\mathrm{m^3/time\,step})}{Q_{total} \ (\mathrm{m^3/time\,step})} \tag{4.4}$$

where units are displayed in parentheses, and Q_{trench} is the flux through the trenches such that

$$Q_{trench}(\mathrm{m^3/time\,step}) = area\,of\,trenches(\mathrm{m^2}) \times recharge(\mathrm{m/time\,step}) \tag{4.5}$$

Q_{total} is the total flux through the part of the site where waste is buried. It is equal to the flux through the trenches and the flux through the areas between the trenches. For this site it is assumed to have the relationship

$$Q_{total} = Q_{trench} \div 0.70 \tag{4.6}$$

where 0.70 represents the fraction of the waste disposal area that is comprised of trenches.

For any contaminant, the U.S. Environmental Protection Agency (EPA) sets limits for maximum contamination levels allowable in drinking water. These drinking water limits are used as a reference standard against which steady state isotope concentrations

are compared. For H-3 and U-238, C_0 is calculated and used to compute C_{ss} at the spring (x = 1000 meters). C_{ss} is then compared to the drinking water limit for each isotope. A summary of these results appears in Table 4.2.

The results in Table 4.2 show that concentrations of both H-3 and U-238 are potentially of concern at the spring. For H-3, the 1D analytical model predicts a steady state concentration at the spring to be much greater than the drinking water limit. For U-238, the concentration is close to the drinking water limit and is equal to C_0 since uranium-238 has a long half life. This observation indicates that a small increase in solubility of U-238 would result in a potential steady state concentration at the spring that is above the drinking water limit. Solubility may be affected by temperature, pH, and other factors. Not only does U-238 have a long half life, but it also has a high retardation factor (R = 160), making the isotope travel time to the spring on the order of 10^4 years. This observation may make U-238 less of a concern at the spring, but at distances closer to the site contamination may reach significant levels at shorter times. This initial screening model indicates that both H-3 and U-238 are candidates for further investigation in the 2D numerical model in Chapter 5.

4.1.2 Pulse Input

The pulse input model uses a 2D analytical solution to the advection-dispersion equation for an instantaneous pulse input with longitudinal and transverse dispersivity in a uniform flow field. A detailed discussion of this solution is given in Appendix B. The solution is of the form

$$C_{max}(x) = \max\left\{\frac{M e^{-kt}}{t\beta\sqrt{A_{11}A_{33}}}\exp\left[-\frac{(x-\hat{v}t)^2}{4\hat{v}tA_{11}}\right]\right\} = C(x,t_p) \qquad (4.7)$$

where C_{max} is the peak concentration in Ci/m³, t is the time, t_p is the peak time, k is the decay coefficient, $\hat{v}$ is the retarded velocity, x is the distance, and β is a function of $\hat{v}$ and other factors (see Appendix B). M is the total isotope inventory in the waste trenches in Curies. An expression for the peak time is:

$$t_p = \frac{-1 + \sqrt{1 + \frac{x^2}{\hat{v}A_{11}}\left(k + \frac{\hat{v}}{4A_{11}}\right)}}{2\left(k + \frac{\hat{v}}{4A_{11}}\right)} \qquad (4.8)$$

Using Equations 4.7 and 4.8, for a given distance, C_{max} and the time to the peak, t_p, may be determined. These variables are evaluated with x =1000 meters and assumed values for A_{11} and A_{33}, for the isotopes identified above as a pulse input isotopes. The assumptions and results are summarized and compared to the drinking water limits in Table 4.3.

The results in Table 4.3 show that while no isotopes have predicted peak concentration levels above the drinking water limits, three isotopes, I-129, Sr-90, and Tc-99 have concentrations within three orders of magnitude of the limits. Strontium-90 (Sr-90) is of particular interest because of its short half-life. Not only is Sr-90 concentration reduced by dispersion and dilution, during its transport from the site to the

Table 4.2 Summary of parameters for step input screening model.

isotope	k (1/year)	isotope travel time (years)	κ (1/m)	C_0 (Ci/m^3)	C_{ss} (Ci/m^3)	drinking water limit (Ci/m^3)
H-3	5.64E-02	58	3.03E-03	1.08E+00	5.22E-02	1.00E-03
U-238	1.55E-10	9241	1.43E-09	1.72E-07	1.72E-07	3.00E-07

Table 4.3 Summary of parameters for pulse input screening model.

isotope	k (1/year)	R	A_{11} (m)	A_{33} (m)	t_p (years)	C_{max} (Ci/m^3)	drinking water limit (Ci/m^3)
Am-241	1.60E-03	6361	100	0.25	23566	8.23E-41	2.00E-08
Co-60	1.32E-01	40.8	100	0.25	207	1.60E-24	3.00E-06
Cs-137	2.30E-02	1988	200	0.25	2479	1.46E-52	1.00E-06
I-129	4.33E-08	20.9	100	0.25	988	1.30E-08	2.00E-07
Sr-90	2.41E-02	58.2	242	0.25	358	3.57E-10	5.00E-07
Tc-99	3.24E-06	5.0	145.5	0.25	216	3.08E-06	6.00E-05

spring, it is further reduced by radioactive decay. As a result, points between the site and the spring may have concentrations that are several orders of magnitude higher than those predicted at the spring. The 2D numerical model provides the opportunity to evaluate this spatial distribution of Sr-90 over time. I-129 and Tc-99 are both within an order of magnitude of the drinking water limit, according to the results in Table 4.3. Both isotopes have extremely long half lives and do not experience significant decay over their travel to the spring. Technetium-99 (Tc-99) has a peak time at the spring of 216 years, as compared to 988 years for I-129. Additionally, Tc-99 exhibits clay-content dependency of K_d, an aspect that is interesting to model (see Section 4.2). For these reasons, the two isotopes selected for modeling as pulse inputs in the 2D numerical model of Chapter 5 are strontium-90 and technetium-99.

The screening models are a method of selecting contaminants for further evaluation using simple analytical methods. The limitations of these screening models and a comparison of their predictions with the results of the 2D numerical model is discussed in Chapter 5.

4.2 Sorption Dependence and Evaluation

Isotope sorption as characterized by the distribution coefficient, K_d, has been found to vary with any of a number of different soil parameters, depending on the specific isotope. For the isotopes of concern in this analysis, the governing soil parameters are pH and clay content. Strontium-90 K_d has been shown to vary with pH, while technetium-99 K_d is dependent on clay content (Hoeffner, 1985). Although little is known about the dependence of uranium-238 K_d in site soils, the isotope is assumed to exhibit some increased spreading as a result of sorption variability. Tritium is not sorbed, and therefore is not treated in this analysis.

4.2.1 Strontium-90: Sorption Dependence on pH

Measurements of pH from soil and water samples at the hypothetical site and at another site with similar soils have been compiled from several different sources (Goode, 1986; Cahill, 1982), and are shown in Figure 4-1 as a function of sample depth. Since this figure shows an equal scattering of the data for different depths, the sample set is assumed to be representative of the entire aquifer. The pH data set presented in Figure 4-1 is shown in a histogram in Figure 4-2. The high values of pH are probably due to contamination of the samples by dissolution of grout around well bores, and therefore are assumed not to reflect accurately *in situ* pH. A statistical analysis of the pH data gives a mean pH ($\overline{pH}$) of 5.57, and a standard deviation of pH (σ_{pH}) to be 0.88. Samples with a pH greater than 8.5 are not included in the statistical calculations.

Hoeffner (1985) shows a correlation between strontium-90 K_d and pH in coastal plain sediments, according to Figure 4-3. As derived from Figure 4-3, if pH is taken to be normally distributed, K_d is therefore lognormal with the relationship

$$\log K_d = a + 1.14\,(pH) \tag{4.9}$$

where a is the intercept, and 1.14 is the slope, as calculated from Figure 4-3. A conversion of this equation into natural logarithms provides

$$\ln K_d = a' + 2.65\,(pH) \tag{4.10}$$

and this yields

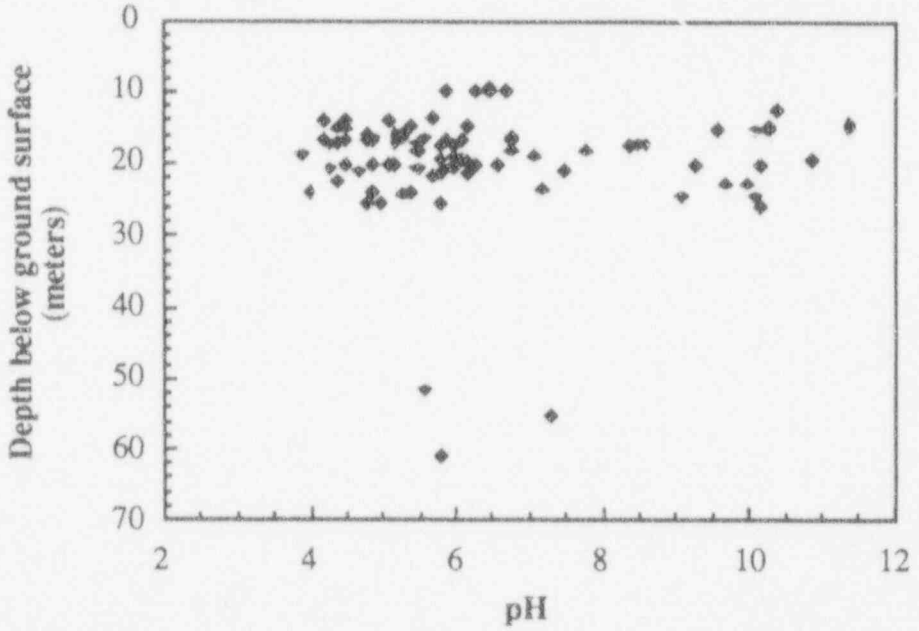

Figure 4-1 Collected values of pH versus depth; measurements from Cahill (1992, tables 8, 9) and Goode (1986).

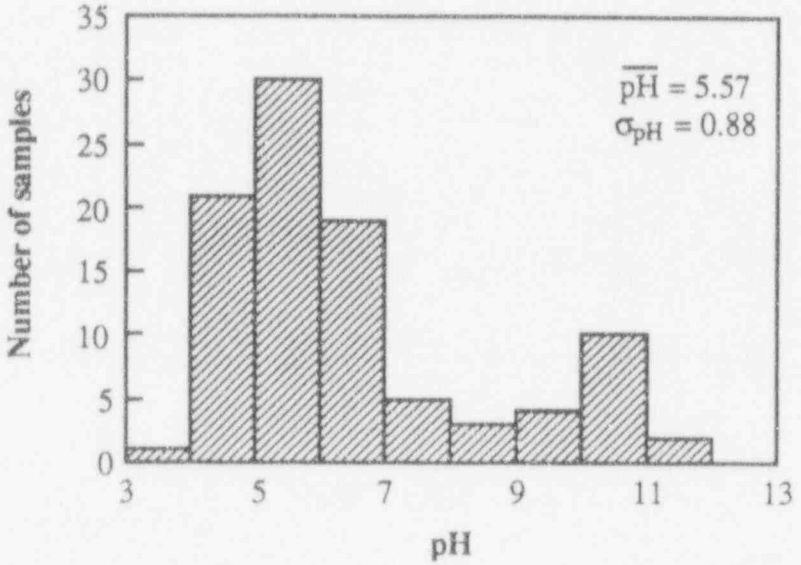

Figure 4-2 Distribution of measured pH values from 95 site water and soil samples; data taken from Cahill (1982, tables 8, 9) and Goode (1986).

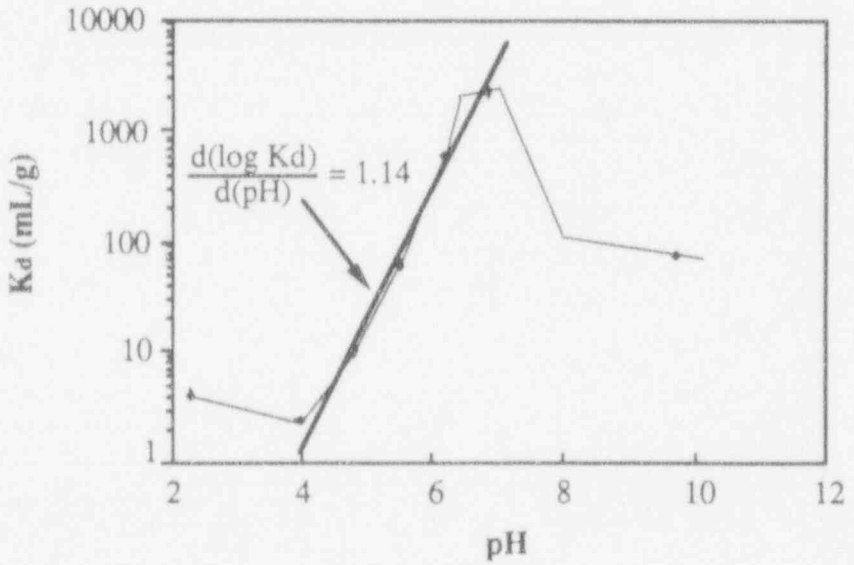

Figure 4-3 Relationship of site pH variation to strontium-90 K_d; reproduced from Hoeffner (1985, figure 5).

$$\sigma_{\ln K_d} = 2.65\,\sigma_{pH} \tag{4.11}$$

In Figure 4-3, for $\overline{pH} = 5.57$, the corresponding value of K_d is 60 mL/g. Because K_d is lognormal, this value is the geometric mean of K_d, $K_{dG} = 60$ mL/g, where $K_{dG} = E[\ln K_d]$. Additionally, for $\sigma_{pH} = 0.88$, the relationship in Equation 4.11 can be used to find $\sigma_{\ln Kd} = 2.3$. The definition of a lognormal distribution may be used to determine $\overline{K}_d$ and σ_{Kd} from K_{dG} and $\sigma_{\ln Kd}$, according to the following:

$$\overline{K}_d = K_{dG}\, e^{\sigma^2_{\ln Kd}/2}\ ; \qquad \frac{\sigma^2_{K_d}}{\overline{K}_d^2} = e^{\sigma^2_{\ln Kd}} - 1 \tag{4.12}$$

Using the values of $\overline{K}_d$ and σ_{Kd} as calculated above, the coefficient of variation for K_d ($\sigma_{Kd}/\overline{K}_d$) is calculated to be 14.9, indicating that $\overline{K}_d$ has a value close to 900 mL/g. This value is extremely high and is probably unreasonable given other knowledge about K_d (Pietrzak and Dayal, 1982). It is not known how representative of actual *in situ* aquifer conditions the pH data may be, but it is evident that the choice of $\sigma_{\ln Kd}$ will greatly impact the calculation of the increase in macrodispersivity, as seen in Equation 3.9.

For purposes of illustration, is assumed that the coefficient of variation for K_d is 1.5. This reflects a more moderate value for σ_{pH}, on the order of 0.41. Using these new assumptions and a value for $K_{dG} = 8$ mL/g as proposed for Sr-90 by Campbell (1992), the effect of K_d variability on longitudinal macrodispersivity may be determined from Equation 3.9. There is no information on the correlation between pH and ln$K$. It is arbitrarily assumed for this case that there is no correlation, *i.e.*, in Equation 3.9, $\zeta = 0$. The longitudinal macrodispersivity enhancement is calculated on the basis of this assumption. A summary of the relevant parameters is given in Table 4.4.

As can be seen in Table 4.4, even a relatively moderate variability in K_d has a large effect on longitudinal macrodispersivity enhancement. In the case of strontium-90, the increase of A_0 by a factor of 9.7 will result in a large longitudinal spreading of the plume and will affect the travel time of the leading edge of the plume, as confirmed by the numerical model results in Chapter 5.

4.2.2 Technetium-99: Sorption Dependence on Clay Content

Measurements of clay content from site soil samples are shown in Figure 4-4 (Cahill, 1982). A statistical analysis of this data set gives a mean, $\overline{\%clay} = 30\%$, and the standard deviation, $\sigma_{\%clay} = 10$.

For technetium-99 (Tc-99), Hoeffner (1985) demonstrates a positive correlation of clay content and K_d (see Figure 4-5), however, there are insufficient data to ascertain an exact relationship between *%clay* and Tc-99 K_d. If a relationship could be determined, $\overline{K}_d$ and σ_{Kd} for Tc-99 would be calculated in the same manner used in the evaluation of K_d for Sr-90. Since no actual values are available, values are assumed arbitrarily for the purposes of illustrating the analysis. Using a value of Tc-99 $\overline{K}_d = 1$ mL/g (Campbell, 1992), and assuming that $\sigma_{Kd}/\overline{K}_d = 1.0$, the effect of K_d variability on longitudinal macrodispersivity may be determined from Equation 3.9 in the same manner as shown above for strontium-90. In contrast to pH, clay content is correlated with hydraulic conductivity. A high percentage of clay in the soil corresponds to a low hydraulic conductivity. For this reason, the correlation fraction, ζ, in Equation 3.9 is assumed to be 0.5. The relevant parameters are summarized in Table 4.5.

Table 4.4 Parameters used to calculate effect of Strontium-90 K_d variability on increase in longitudinal macrodispersivity.

σ_{pH}	$\overline{K}_d$ (mL/g)	$\sigma_{Kd}/\overline{K}_d$	$\overline{R}$	$\sigma_R/\overline{R}$	ρ_b (g/mL)	n	σ_{lnK}	γ	ζ	λ_n/λ_1	A_{11}/A_0
0.41	14.42	1.5	58.3	1.47	1.59	0.4	2.0	4.0	0.0	1	9.7

Table 4.5 Parameters used to calculate effect of Technetium-99 K_d variability on increase in longitudinal macrodispersivity.

$\overline{K}_d$ (mL/g)	$\sigma_{Kd}/\overline{K}_d$	$\overline{R}$	$\sigma_R/\overline{R}$	ρ_b (g/mL)	n	σ_{lnK}	γ	ζ	λ_n/λ_1	A_{11}/A_0
1	1.0	5.0	0.8	1.59	0.4	2.0	4.0	0.5	1	5.82

Table 4.6 Summary of isotope parameters that are used in the numerical model.

isotope	decay coefficient (1/year)	$\overline{K}_d$ (mL/g)	C_0 (Ci/m³)	M (inventory) (Ci)	ζ	A_{11}/A_0	A_{11} (m)	A_{33} (m)
H-3	5.64E-02	0	1.08E+00			1	25	0.25
U-238	1.55E-10	40	1.72E-07		0	2.96	74	0.25
Sr 90	2.41E-02	14.4		3.33E+05	0	9.69	242	0.25
Tc 99	3.24E-06	1		1.21E+02	0.5	5.82	145.5	0.25

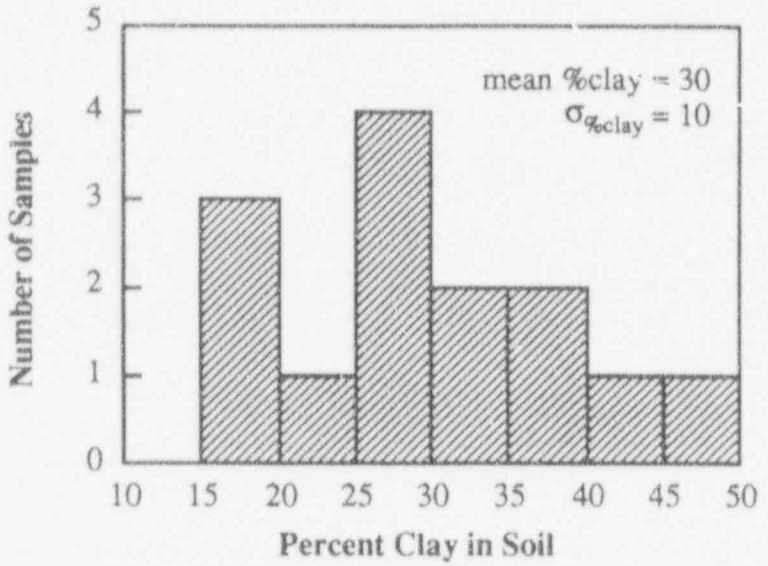

Figure 4-4 Distribution of measured values of clay content from 14 site soil samples; data taken from Cahill (1982, table 11).

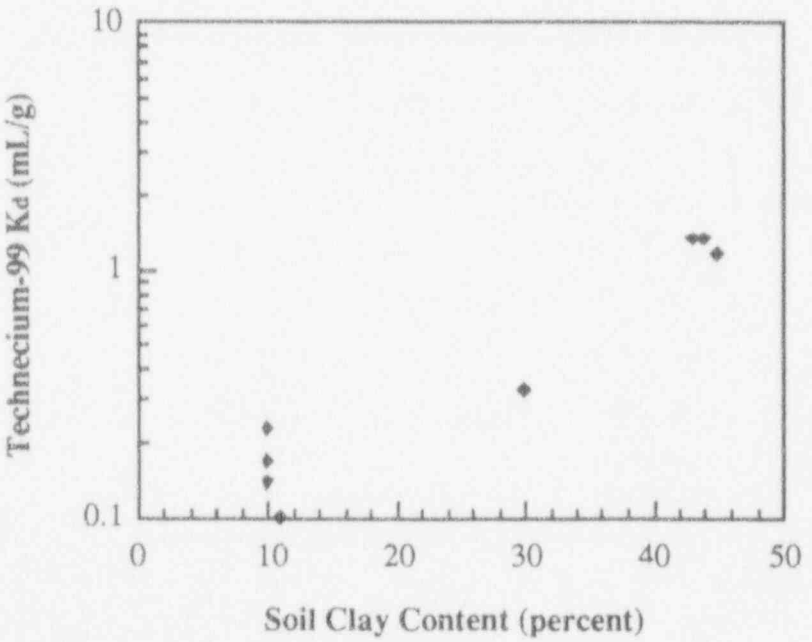

Figure 4-5 Relationship of site clay content variation to technetium-99 K_d; data taken from Hoeffner (1985, table XI).

4.2.3 Uranium-238: Macrodispersivity Enhancement

At the hypothetical site, the dependency of uranium-238 (U-238) K_d on soil properties is not known. However, it is assumed that U-238 does exhibit some longitudinal macrodispersivity enhancement due to sorption variation. Using a value of U-238 $\overline{K}_d$ to be 40 mL/g, as given by Campbell (1992), and assuming $\sigma_{K_d}/\overline{K}_d = 0.7$ and $\zeta = 0$, the macrodispersivity enhancement is calculated from Equation 3.9. Following the procedure for Sr-90 and Tc-99, this calculation gives $A_{11}/A_0 = 2.96$ for U-238 in site soils.

A final summary of the important properties of all four isotopes is provided in Table 4.6.

4.3 Discussion

The assumptions and the uncertainties in the above analysis emphasize the need for a more comprehensive method of data collection and evaluation. An important conclusion of this analysis is that while it is possible to develop crude estimates of K_d variation from a derived relationship with a soil parameter, it would be more meaningful to measure K_d variations directly. If laboratory tests for K_d for each isotope are conducted on the same samples as are tests for K, not only would it result in a quantification of K_d variability, it would also determine the correlation between K_d and K for each isotope of concern. Each sample would then be a single data point in Figure 3-8, and a precise value for ζ could be derived for each isotope.

The calculated values of macrodispersivity enhancement in this chapter are tentative, at best. They are not meant to give precise levels of enhancement, but are calculated to illustrate the process of macrodispersivity enhancement parameter estimation discussed in Subsection 3.2.3, and to serve as input parameters to the 2D numerical model in Chapter 5. It is hoped that modelers who traditionally use an unenhanced value of longitudinal macrodispersivity will recognize the magnitude of the effect of enhancement on model results, and that this approach will serve as the basis for future model input parameters.

CHAPTER 5
NUMERICAL MODELS

The hydraulic parameters determined from the theory in Chapter 3 and the isotope parameters from Chapter 4 are entered into traditional numerical models based upon the hypothetical site characteristics in Chapter 2. These models illustrate the effects of stochastic parameter estimation on isotope transport simulation.

The models are created and analyzed using a commercially available finite element flow and transport computer code, SUTRA Mac, Version 1.3 (Geraghty & Miller, Inc., Reston, VA; see Voss, 1984). The program allows for 2D anisotropic transient flow and transport modeling with sorption and decay. Although the unsaturated zone is not included in the models in this report, the program does contain the capability to include unsaturated flow as well.

Using this program, two models are configured to simulate two separate transport scenarios. The first model is a 2D rectangular vertical cross-section representing downgradient flow from the hypothetical waste site to the spring (see Figure 2-1). The second model is a 2D radial wedge representing the contribution of flow from the site in the direction of a hypothetical municipal pumping well located near the city in Figure 2-1.

5.1 Rectangular Model

The hypothetical waste site is located upgradient from the spring, with an indication that most of the water entering the site as recharge will flow downgradient to the spring. The 2D rectangular model from the site to the spring is typical of a LLW site local groundwater model. Analysis using this model includes an evaluation of contaminant transport to the spring and to a hypothetical observation well at the property boundary for all four isotopes identified in Chapter 4.

5.1.1 Model Configuration

The 2D rectangular model is a one meter-wide vertical slice across the center of the waste site and along the 1300-meter downgradient path to the spring (see Figure 5-1). The 2D model represents a conservative estimate of the actual 3D problem, since it does not account for concentration dilution due to horizontal transverse dispersion. However, because the width of the waste site (about 400 meters) is significant in comparison to the overall problem scale (1300 meters), it is expected that even in a 3D model, horizontal transverse dispersion would play a minimal role in reducing concentrations at the center of the site. The gradients in Zones 1, 2, and 3 are all in the direction of the spring, so that the transverse advective flux neglected in a 2D representation of a 3D system will also be minimal (see Figure 5-1).

As shown in Section 3.3, the unsaturated zone is expected to play a minimal role in the transport problem. The 2D rectangular model neglects the unsaturated zone and uses the water table as the upper fixed-head boundary. The lower boundary is provided by the thick clay aquitard mentioned in Chapter 2. Water table heights are measured

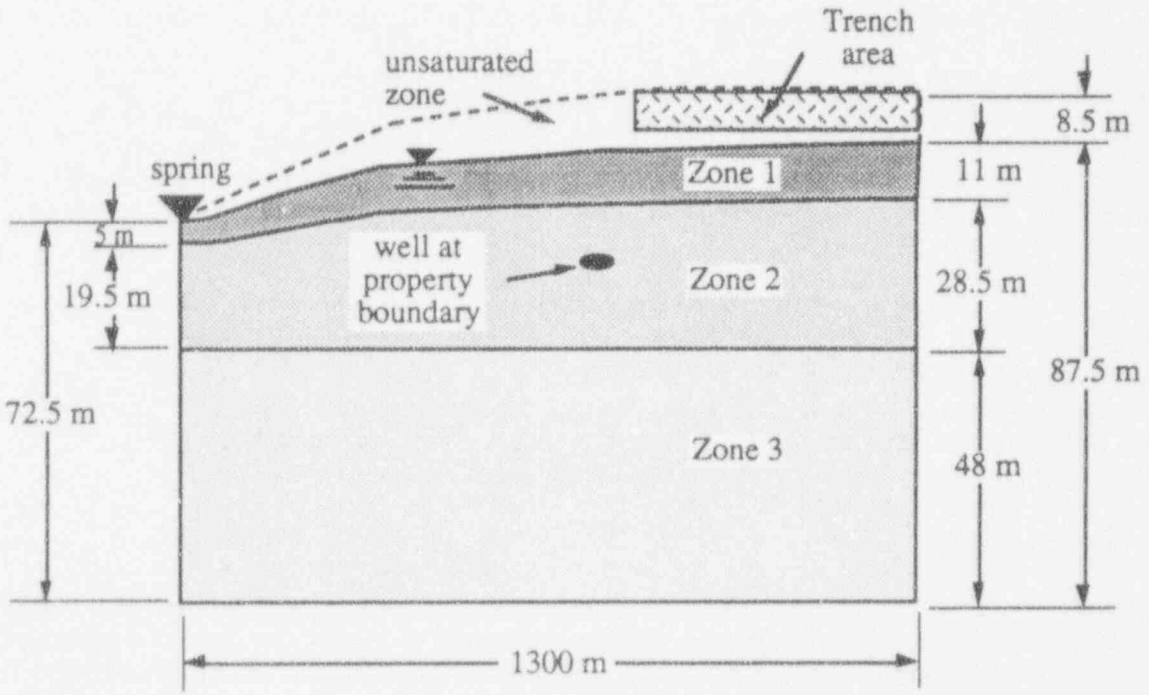

Figure 5-1 Cross section of 2D rectangular model showing relative thickness of zones; vertical scale is greatly exaggerated.

relative to the lower boundary. Figure 5-1 shows an idealized cross-section for the 2D rectangular model.

Because the waste site is located near a groundwater divide, the upstream boundary of the model is a no-flow boundary. Likewise, the spring is a local flow divide since it receives influx from the groundwater on either side. For this reason, the downstream boundary at the spring is also a no-flow boundary. This configuration assumes that all the water that enters the model as recharge will be discharged at the spring. The validity of this assumption is dependent on the extent to which Zone 3 receives local recharge and contributes to discharge at the spring. If Zone 3 does not have a true groundwater divide at the site, some of the flow in Zone 3 may be upstream regional flow. At the same time, not all of the flow in Zone 3 may discharge to the spring. The effect of this lower zone flow-through would be to cause dilution in contaminant concentrations, and to reduce the travel time of some local circulations. An approach that could incorporate this possibility would be a model with a larger horizontal extent that takes into consideration regional as well as local flow patterns. Because there is little information to indicate that Zone 3 does not have a groundwater divide, the boundary conditions of the 2D rectangular model reflect the assumption that the divide exists for all zones.

The application of a finite element model to a particular problem involves the discretization of the problem with a mesh. The mesh for the 2D rectangular model, with appropriate boundary conditions, is shown in Figure 5-2. The mesh is comprised of 600 elements and 651 nodes. The horizontal nodal spacing is 43.3 meters, and the average vertical nodal spacing is 4 meters. There are twenty elements in the vertical direction, with two in Zone 1, six in Zone 2, and 12 in Zone 3. The depiction of the mesh in Figure 5-2 shows an enlarged vertical scale.

As an alternative to specifying the recharge flux, a net recharge is induced by varying the hydraulic head along the water table. By specifying a curved water table shape down to the spring, all the recharge is forced to discharge at the spring. An adjustment of the hydraulic conductivity (as discussed in Subsection 3.2.2) is used to calibrate the magnitude of the average net induced recharge with the assumed site recharge of 0.4 meters/year from Chapter 2. A comparison of the implied discharge to the spring with available streamflow data (Cahill, 1982, figure 9) provides further substantiation of the flow model. The model head pattern is shown in Figure 5-3, and the model flow pattern is shown in Figure 5-4.

5.1.2 Results

Simulations are run using the 2D rectangular model with each of the four isotope contaminants as inputs. For tritium and uranium-238, the input to the model is a steady state concentration flux into the portion of the model that bisects the trench area (see Figure 3-2). For strontium-90 and technetium-99, the input to the model is a short pulse of concentration at the trench area, followed by a continuous inflow of uncontaminated water.

An observation well is placed at the site property boundary at a depth of about 30 meters below the ground surface (see Figures 5-1 and 5-2). This well is characteristic of local private water supply wells that could be located close to the waste site property. The observation well is used to monitor the magnitude and travel time of contaminants that reach the property boundary.

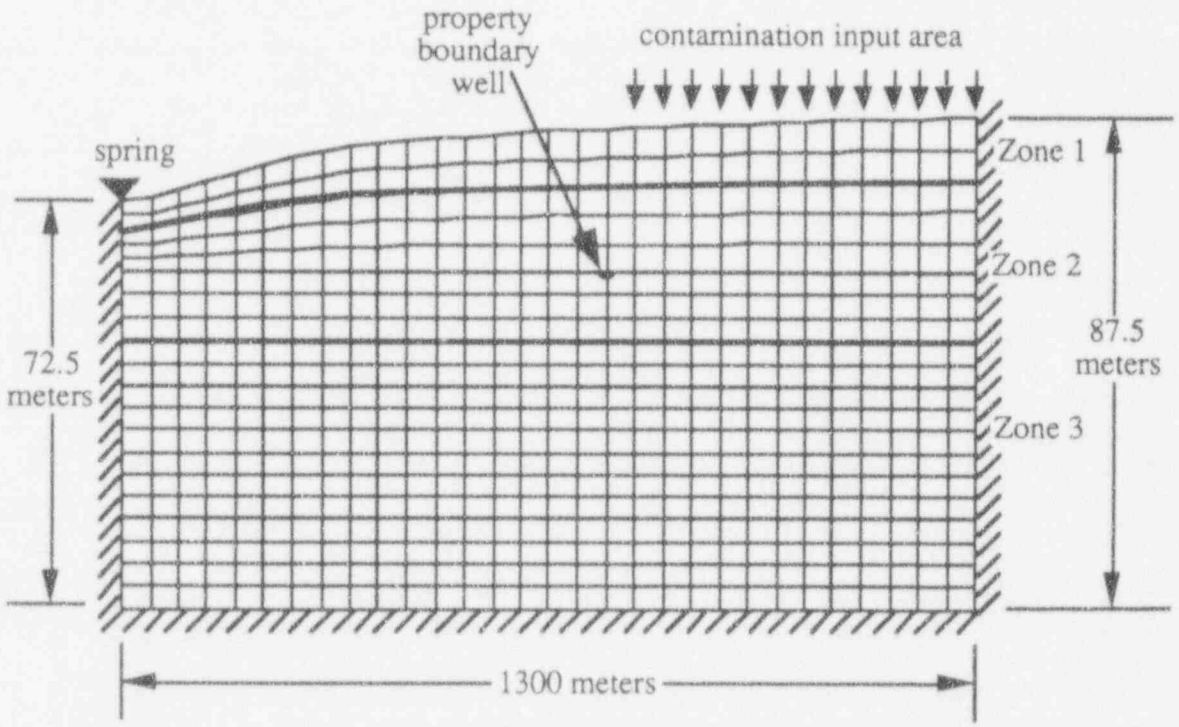

Figure 5-2 Mesh and no-flow and fixed-head boundary conditions used in 2D rectangular finite element model; vertical scale is greatly exaggerated.

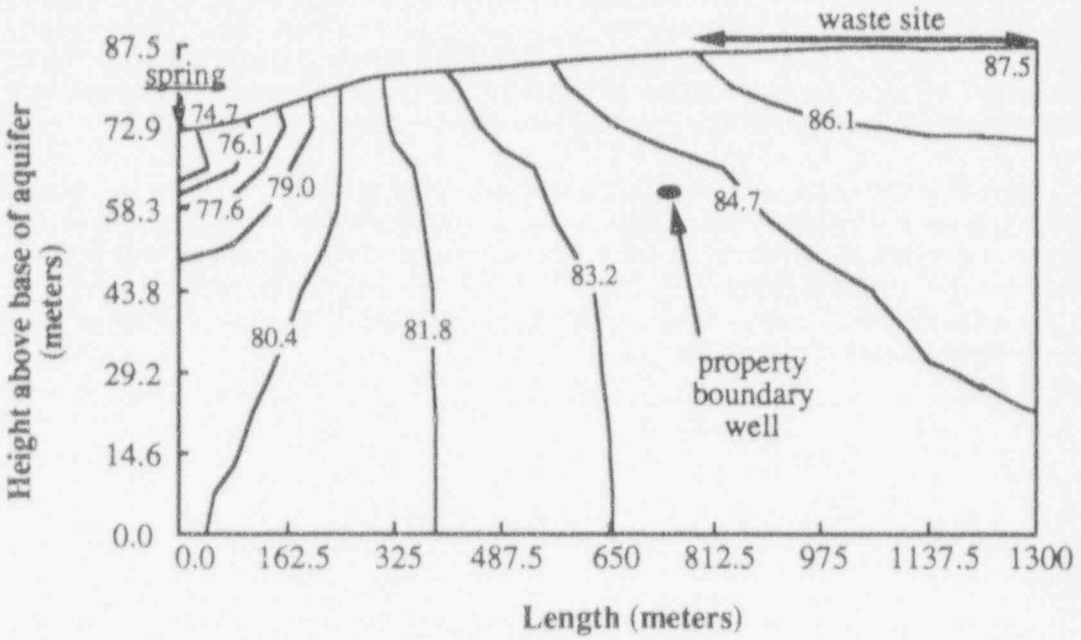

Figure 5-3 Lines of constant head for equal head drops for the 2D anisotropic rectangular model; vertical scale is greatly exaggerated.

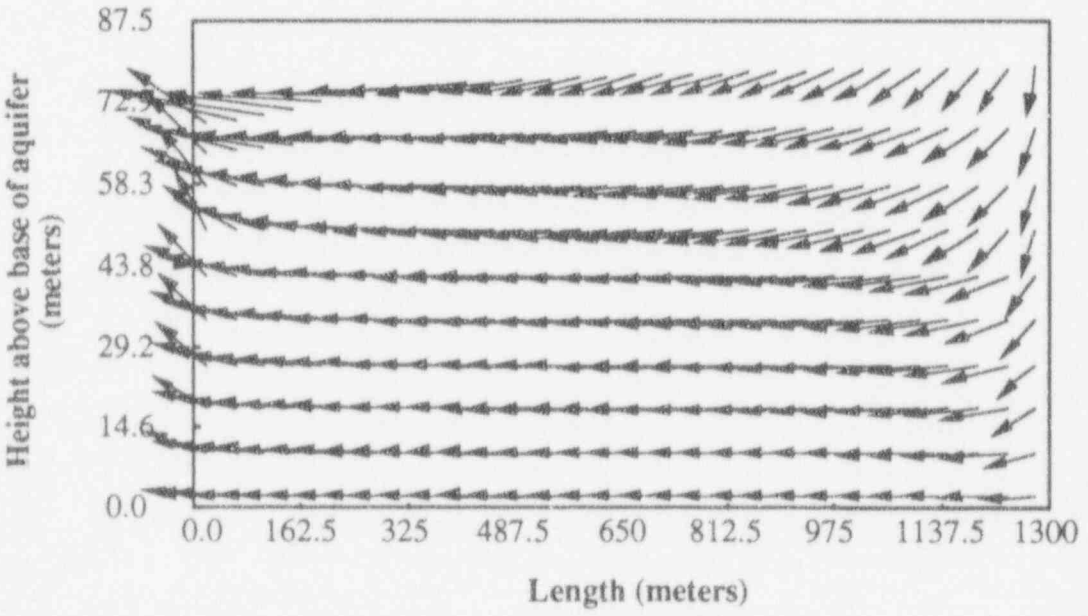

Figure 5-4 Flow pattern for 2D rectangular model with velocity vectors at center of elements. Arrows at downstream boundary indicate flow towards, not flow through impermeable boundary; vertical scale is greatly exaggerated.

Concentration curves at the property boundary well and at the spring are provided for each isotope. Additionally, concentration contours in the model cross-section are shown for the time of peak or steady state concentration at both the property boundary well and at the spring. These contours demonstrate the spatial extent of concentration at the given time. The results are displayed by isotope in Figures 5-5 to 5-12.

The minimum contour levels shown in the contour plots for H-3 (Figure 3-6) and for Sr-90 (Figure 3-10) are the drinking water limits, as discussed in Subsection 4.1.1. All concentration levels displayed in these figures are above the drinking water limits. Since neither the concentrations of Tc-99 or U-238 are ever above the drinking water limits, the concentration contours in Figure 5-8 and Figure 5-12 represent the upper range of concentration present for each isotope.

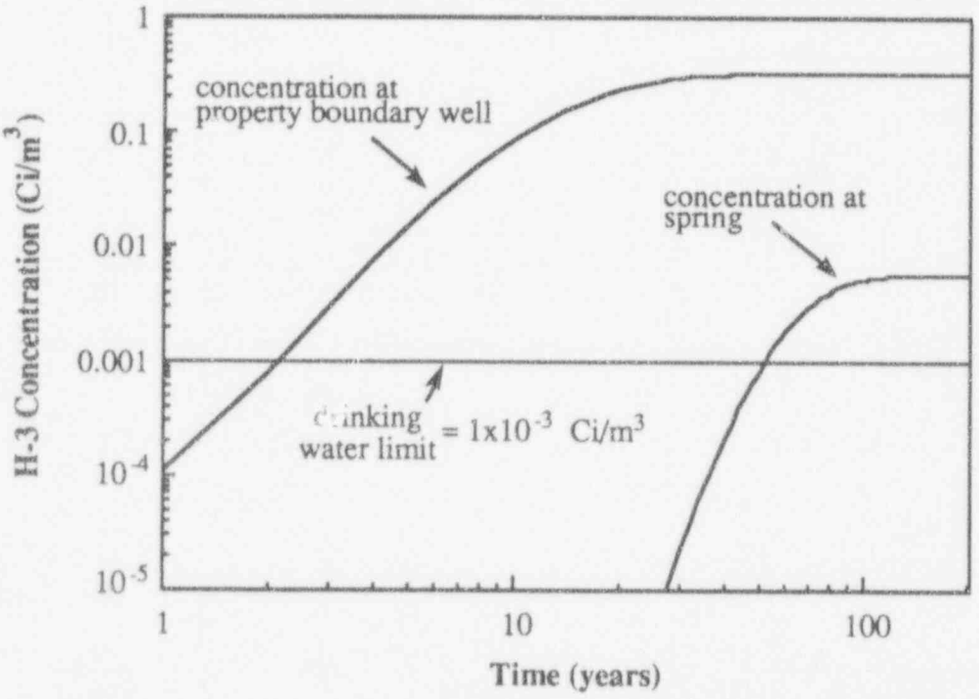

Figure 5-5 Comparison of concentration breakthrough curves for H-3 at spring and at property boundary well.

a) H-3 at 50 years

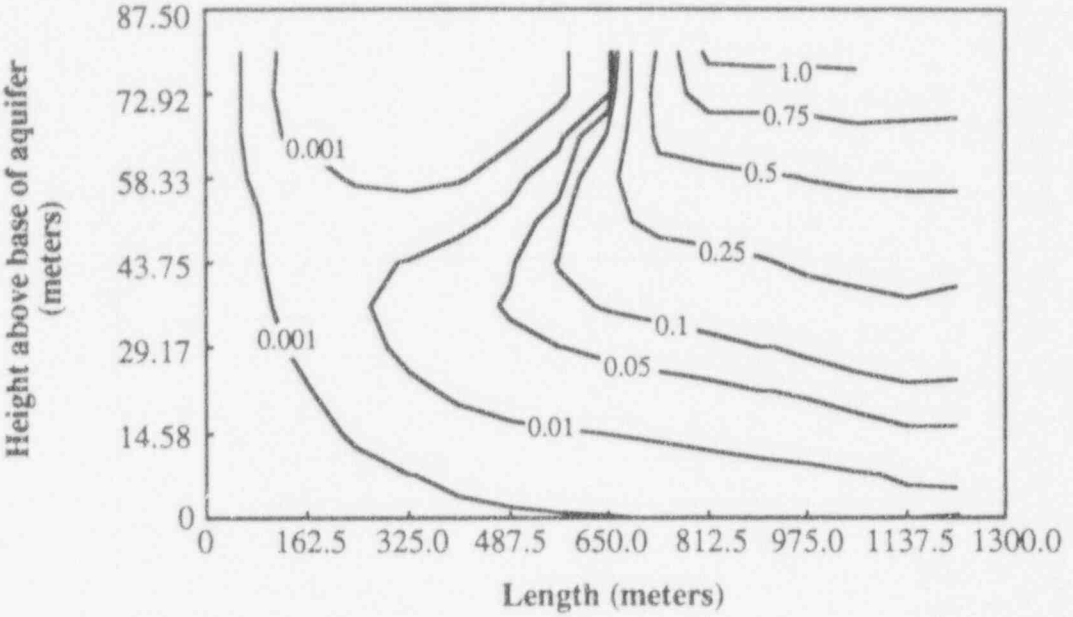

b) H-3 at 150 years

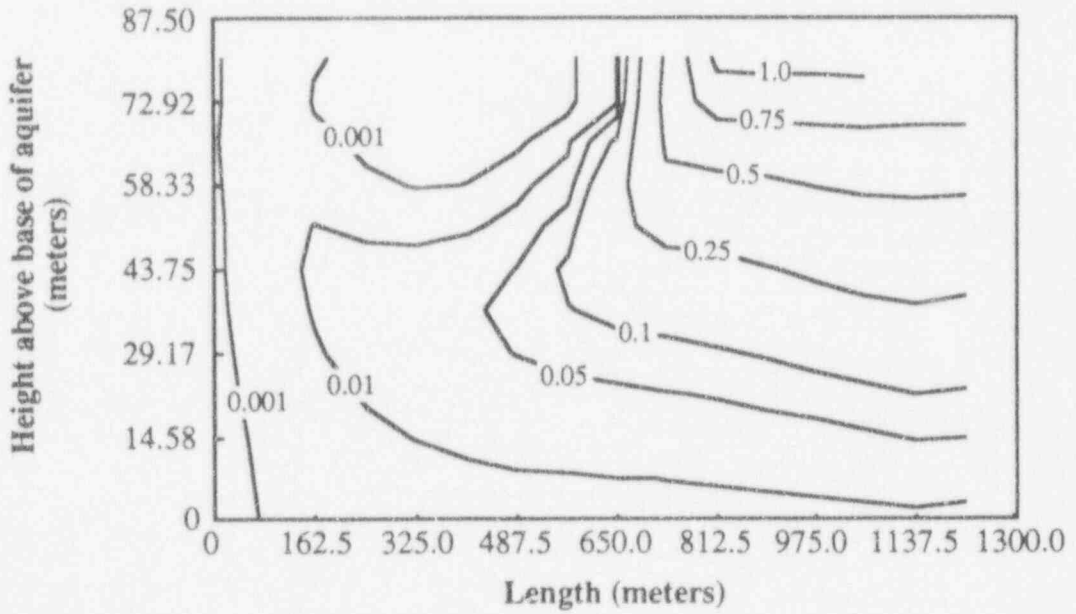

Figure 5-6 Concentration contours of tritium at a) 50 and b) 150 years. Vertical scale is greatly exaggerated and contours are in Ci/m^3. Steady-state source concentration is 1.075 Ci/m^3.

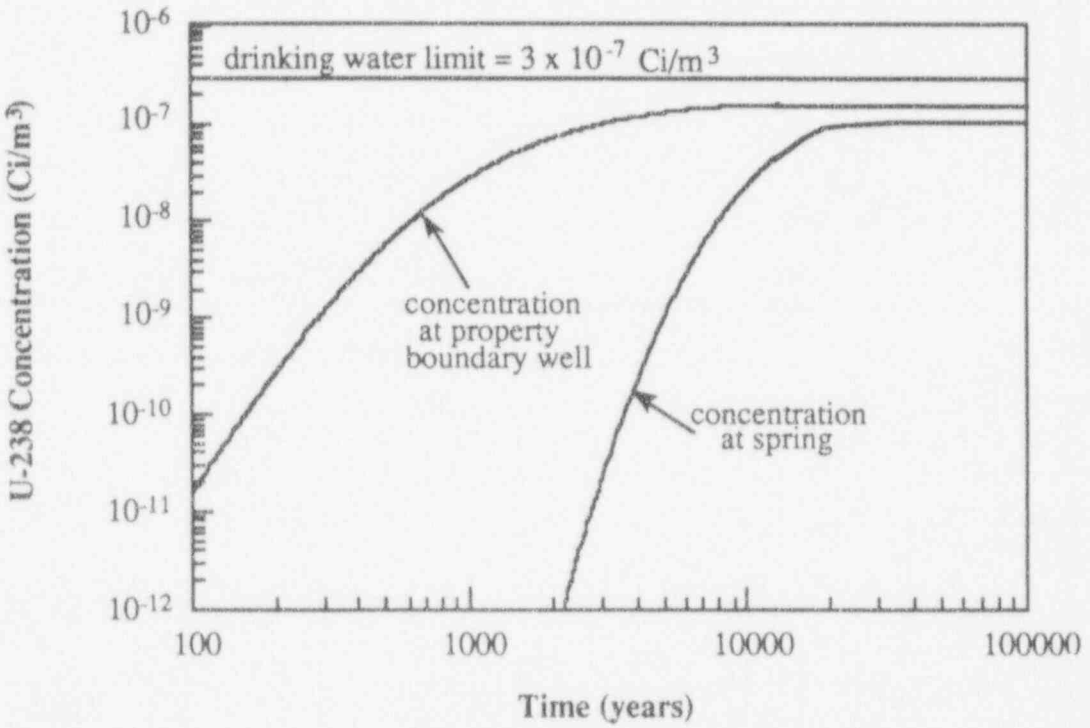

Figure 5-7 Comparison of concentration breakthrough curves for U-238 at spring and at property boundary well.

a) U-238 at 11300 years

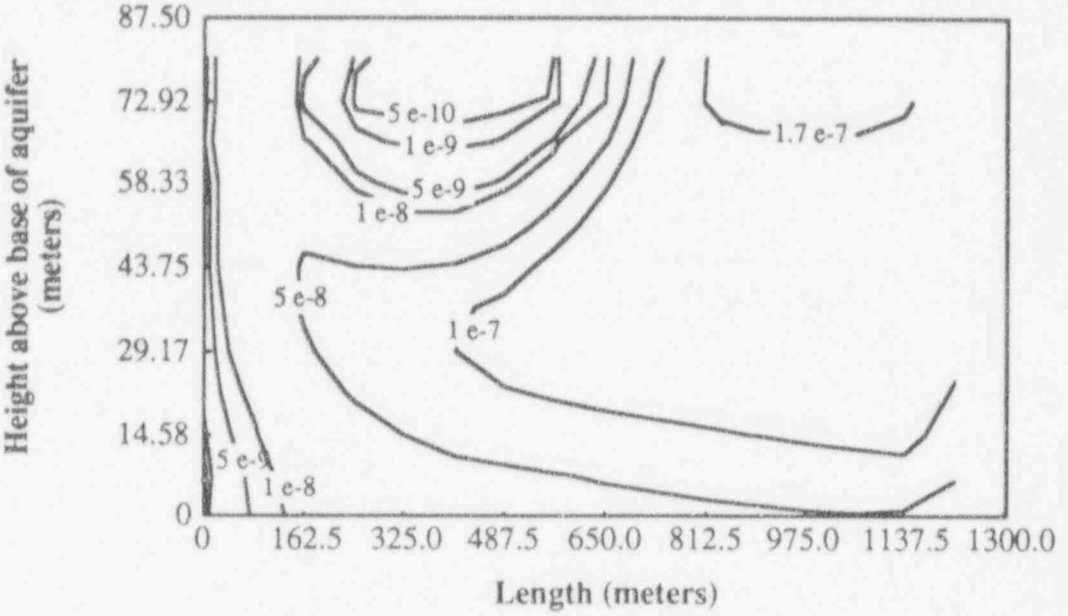

b) U-238 at 14000 years

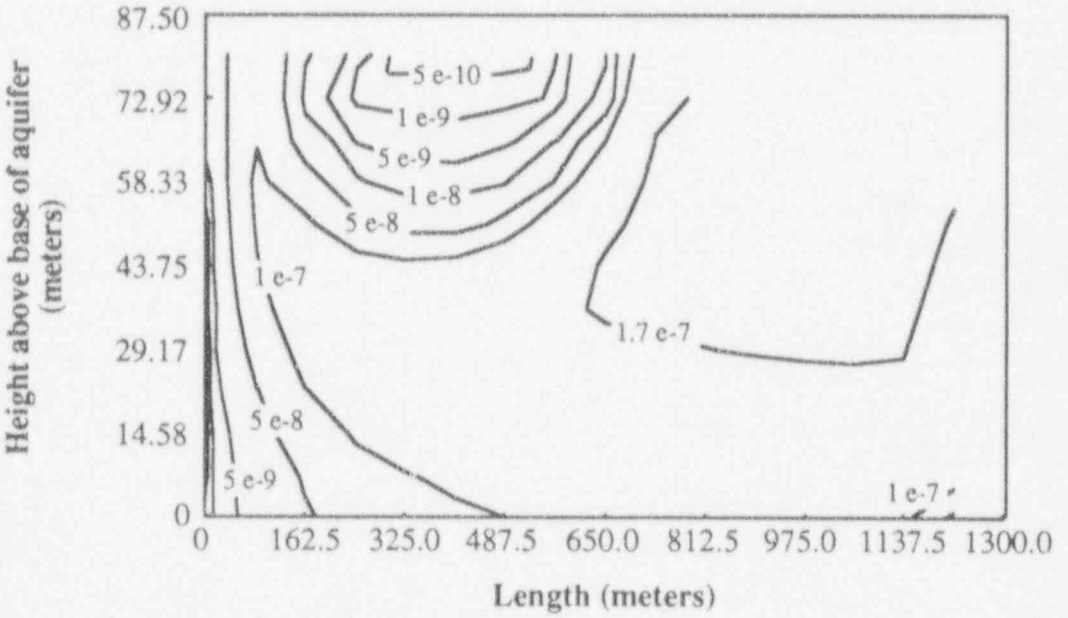

Figure 5-8 Concentration contours of uranium-238 at a) 11300 and b) 14000 years. Vertical scale is greatly exaggerated and contours are in Ci/m³. Steady-state source concentration is 1.72E-07 Ci/m³.

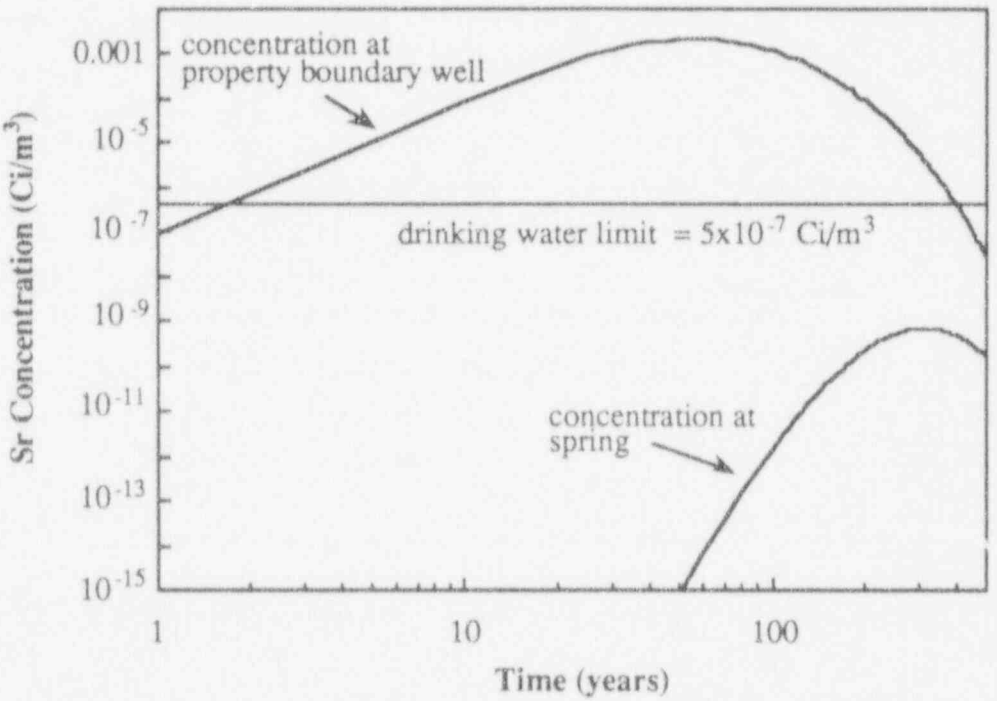

Figure 5-9 Comparison of concentration breakthrough curves for Sr-90 at spring and at property boundary well.

a) Sr-90 at 50 years

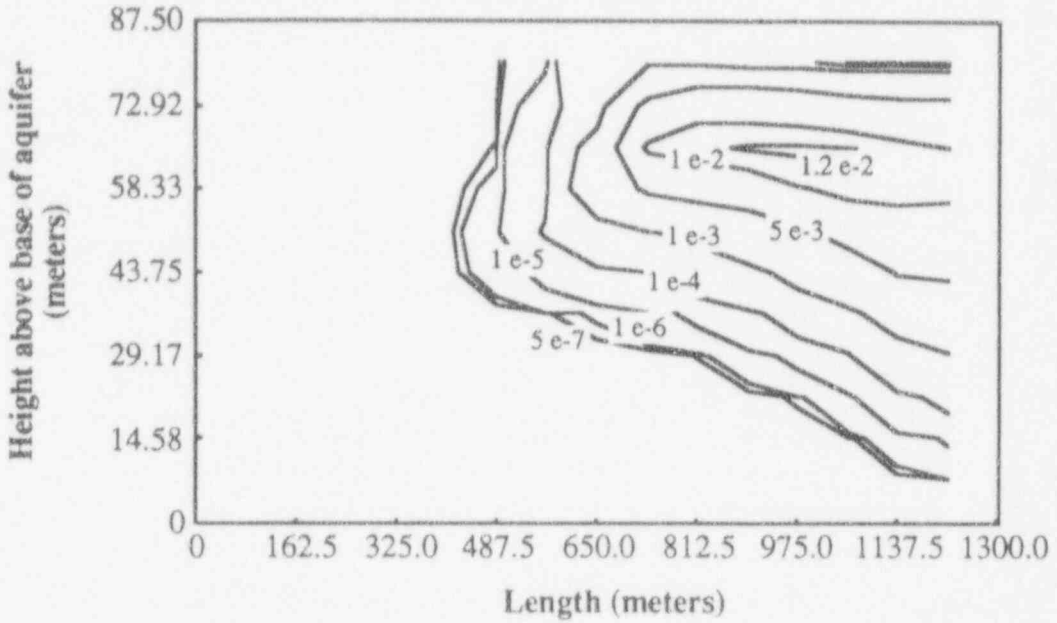

b) Sr-90 at 315 years

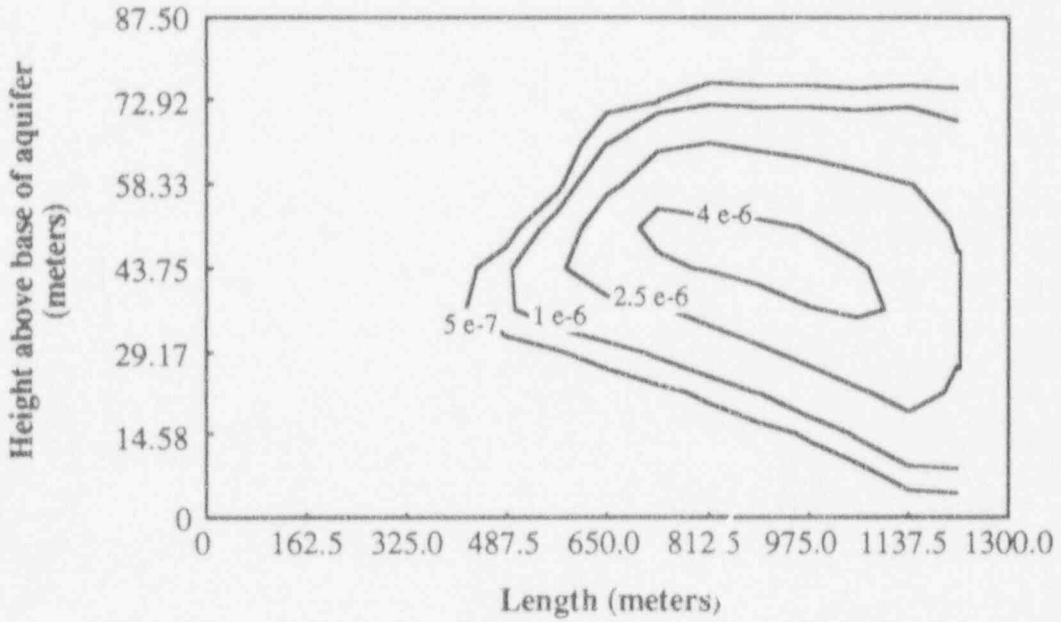

Figure 5-10 Concentration contours of strontium-90 at a) 50 and b) 315 years. Vertical scale is greatly exaggerated and contours are in Ci/m^3.

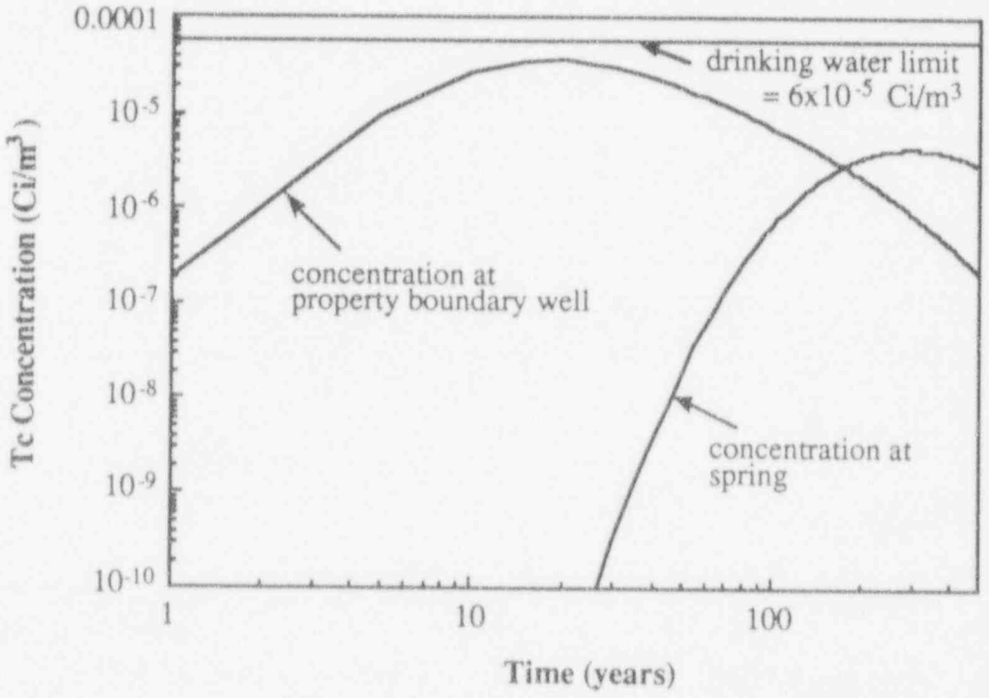

Figure 5-11 Comparison of concentration breakthrough curves for Tc-99 at spring and at property boundary well.

a) Tc-99 at 20 years

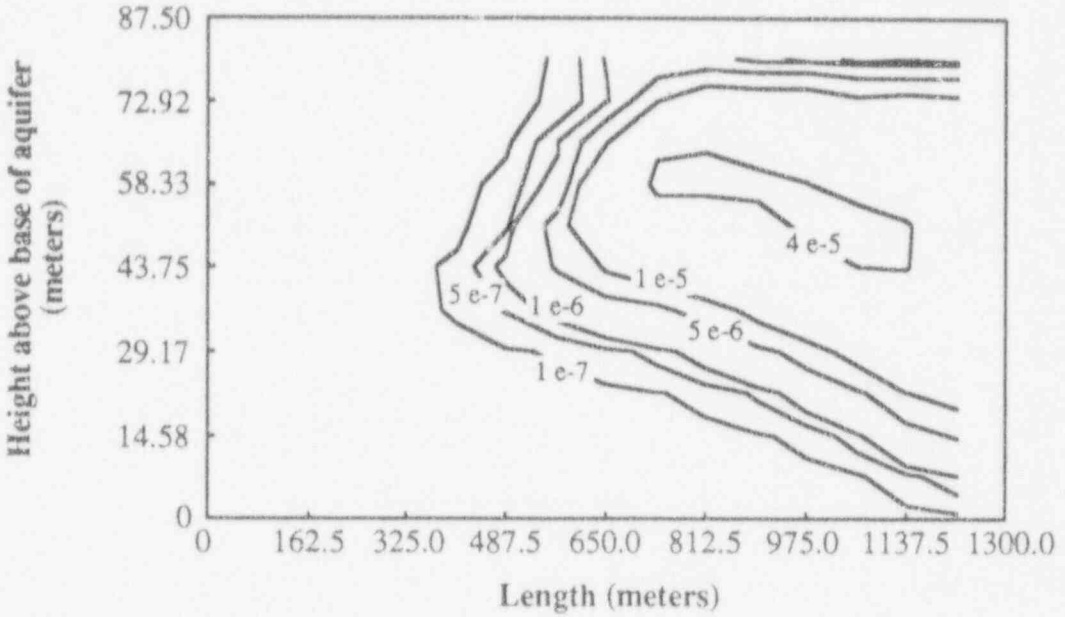

b) Tc-99 at 300 years

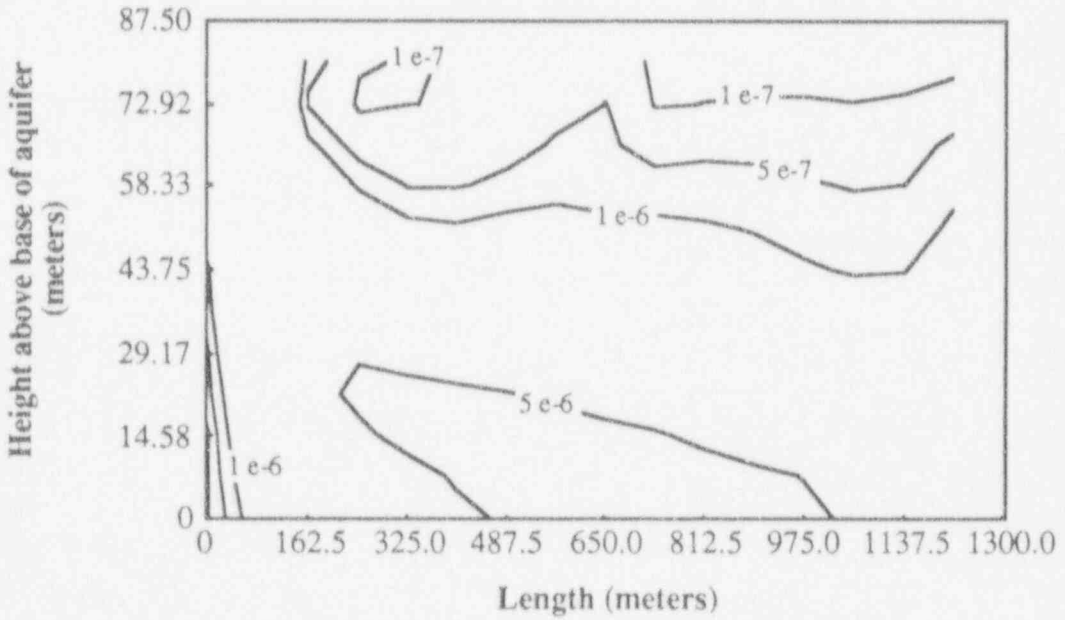

Figure 5-12 Concentration contours of technetium-99 at a) 20 and b) 300 years. Vertical scale is greatly exaggerated and contours are in Ci/m^3.

5.1.3 Discussion and Sensitivity Analysis

In general, the results of the 2D rectangular numerical model follow expected trends. Several points of interest are observed and discussed in the following section.

Although tritium has the shortest half-life of the four isotopes, its lack of retardation and its high solubility result in high concentrations at both the spring and the property boundary well. As a contrast, U-238 experiences almost no decay during the model duration, however it has a high retardation. U-238 will reach significant levels of concentration at both the spring and the property boundary well, but these concentrations will not be present for millennia. Even so, the presence of a relatively high, steady state concentration of U-238 for hundreds of thousands of years could have an effect on future life in the site area, and should not be dismissed as inconsequential.

Tc-99, like U-238, does not experience significant decay during the duration of the model. Tc-99 is affected by dilution and dispersion over time to a greater extent than is U-238, because it is entered as a pulse, and not as a step input. The reduction in the peak concentration from the property boundary well to the spring is a direct result of this dilution and dispersion effect.

Strontium-90 exhibits the most interesting behavior of the four isotopes. Because the half-life of strontium-90 (28 years) is at a comparable order of magnitude as the peak time, augmentations of longitudinal macrodispersivity that increase the velocity of the plume's leading edge also cause an increase in the concentration. Not only does contamination spread further at a given time, but the leading edge of the contamination is higher because it has not decayed as much as it would have if it had spread more slowly. The sensitivity of the strontium-90 results to changes in longitudinal macrodispersivity can be seen through a comparison of breakthrough curves at the spring for 2D numerical simulations with two different values of A_{11}. The enhanced value of A_{11} = 242 meters as calculated in Chapter 4 for strontium-90 is compared with an unenhanced value of A_{11} = 25 meters (see Figure 5-13). The unenhanced value represents the traditional modeling approach, which would not take into consideration the effects of sorption variability on macrodispersivity. The transverse dispersivity, A_{33}, is the same for both cases. Figure 5-13 shows the effects of the different macrodispersivity values. At early time, the undecayed concentration spreading with the higher dispersivity results in a concentration increase of up to ten orders of magnitude. The time at which the peak occurs is almost twice as long for the low dispersivity as it is for the high dispersivity. Due to the significance of dispersivity changes on strontium-90 concentrations, any uncertainties in the determination of A_{11} will greatly affect results. An approach to the evaluation of these uncertainties, and a discussion of their effect is presented in Section 5.3.

5.2 Radial Model

Although the head contours in Figure 2-1 indicate that the mean gradient at the hypothetical waste site is in the direction of the spring, for the purposes of analysis, a second situation is proposed. A large municipal well (or well field) is assumed to be located near the city in the map of Figure 2-1. A second numerical model is designed to evaluate the possible movement of contamination from the site in the direction of this pumping well.

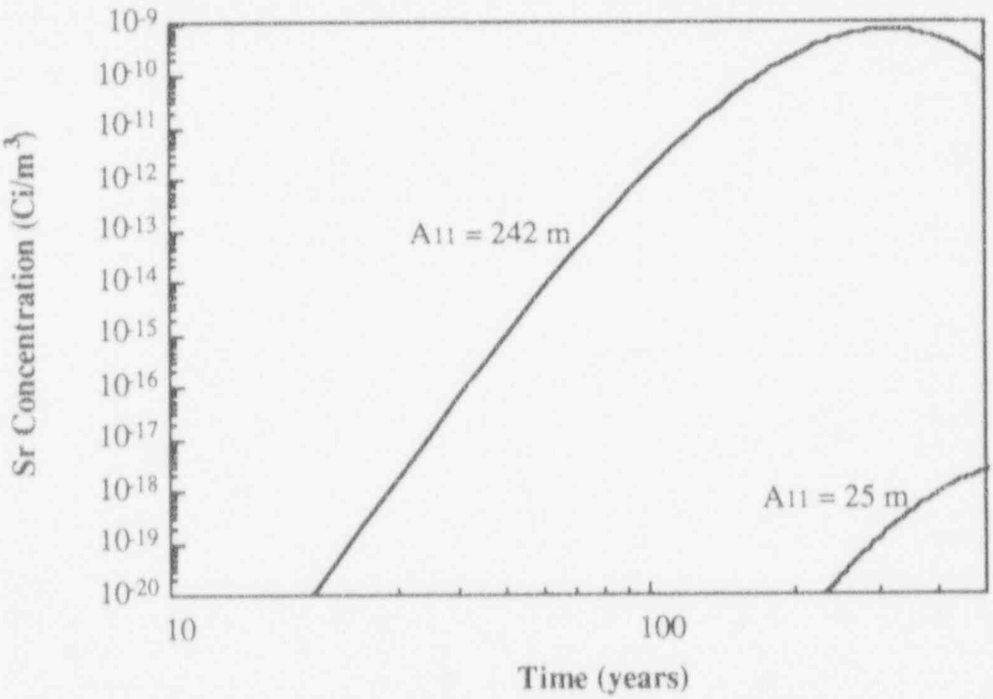

Figure 5-13 Comparison of Sr-90 concentration (Ci/m³) at the spring for numerical simulations of the 2D rectangular model with A_{11} = 242 m and with A_{11} = 25 m.

5.2.1 Model Configuration

Because the model is concerned with the flow to a well, it is appropriate to use a radial coordinate system for the configuration. The flow field is represented by a wedge-shaped mesh, with the well at the center. The wedge extends outward 8400 meters from the well to the site. The maximum width of the wedge is the width of the site. This width represents 15 degrees of the entire circular contribution to the flow at the well.

As described for the rectangular model, the upper boundary of the radial model is the water table, and the lower no-flow boundary is the aquitard. The outer boundary at the site is a no-flow boundary, implying a groundwater divide at the site. The inner boundary at the well is a fixed head boundary over the well screen and a no-flow boundary above the well screen (see Figure 5-14). In moving from the city to the site in Figure 2-1, a river is crossed. Discharge to this river is considered in the radial model. The relative location of this river to the rest of the model is displayed in Figure 5-14. The model configuration assumes that all flow is radial as a result of the pumping well. In reality, local hydraulic circulation may produce non-radial flow that is unaccounted for by this 2D model.

The pumping well is large enough to be a municipal water supply. It is assumed to have a total pumping rate of Q = 0.0241 m³/s (550,000 gallons/day), and to have a radius of 30 meters, representative of a well field. The component of Q that is from the site, Q_s, is given by $Q_s = Q \times 15/360 = 0.001$ m³/s. This is a result of the site flow contribution to the well of 15 degrees. The bottom of the well screen is located 63 meters below the unadjusted water table, with a well screen of 12 meters.

Before the water table height is specified as the fixed head boundary in the radial model, an evaluation is made of the effect of the pumping well on drawdown at the water table. Phillips and Gelhar (1978) provide an expression for drawdown of the water table (ϕ) at any point due to the effects of a short-screened (point source) pumping well. This expression is a function of the pumping rate (Q), the horizontal hydraulic conductivity (K_{11}), the depth of the well (z), and the angle (α) from the vertical at the well to a point on the water table:

$$\phi = -\frac{Q \cos\alpha}{4\pi K_{11} z} \tag{5.1}$$

Using a value of K_{11} = 1.90E-05 m/s for the entire aquifer (see Table 3.1), ϕ is calculated for various locations on the water table. These results for ϕ range from 1.6 meters at the water table above the well, to 0.08 meters of drawdown at the site. The water table heights used in the numerical model reflect the drawdown adjustment as applied to the head measurements from the contours in Figure 2-1.

The drawdown in the well, s, may be estimated using the Jacob approximation for a fully-screened confined aquifer such that:

$$s = \frac{2.3Q}{4\pi T} \log\frac{2.25Tt}{r^2 S} \tag{5.2}$$

where T is the transmissivity, r is the well radius, t is the time (assumed to be one year), and S is the storativity of the aquifer (assumed to be 5.00E-04). The transmissivity is given by $T = K_{11}b$, where b is the thickness of the portion of the aquifer that contributes to

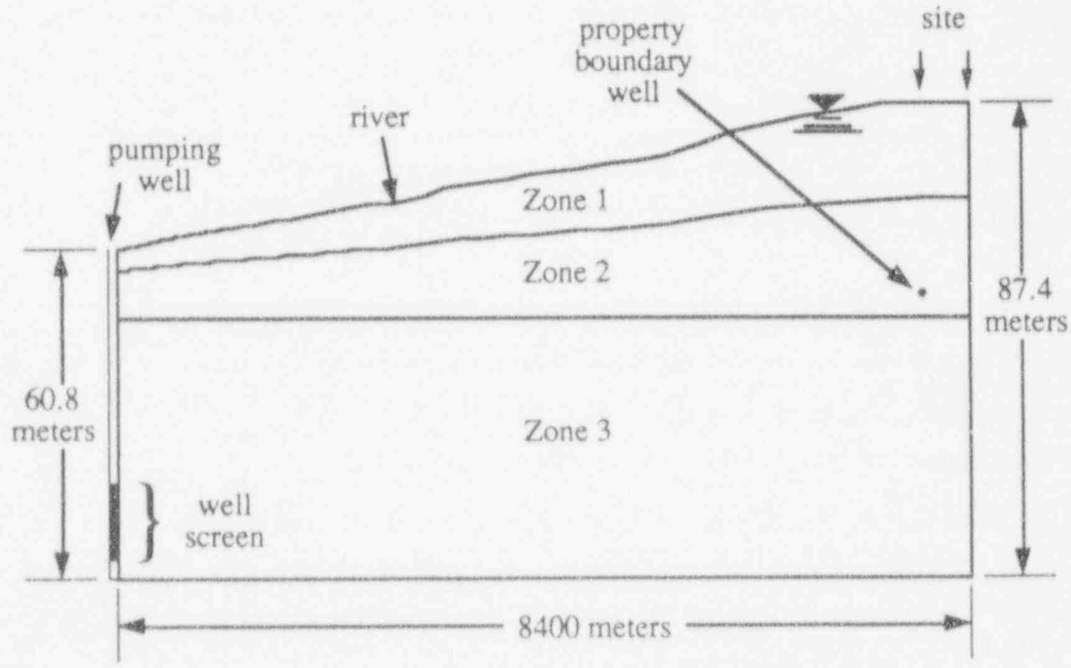

Figure 5-14 Cross-section of the 2D radial model, showing relative thickness of zones and locations of river, pumping well, and property boundary well; vertical scale is greatly exaggerated.

the flow at the well. T is calculated twice (T_1 and T_2), using two different assumptions, for comparison. The first assumption is that flow to the well is only from the portion of the aquifer at the height of the well screen. T_1 is calculated using the horizontal hydraulic conductivity of Zone 3, K_{11} = 3.0E-05 m/s, and b=12 meters (the well screen length). T_1 is calculated to be 1.14E+04 m²/yr. The second assumption is that the entire saturated aquifer width contributes to flow at the well. The horizontal hydraulic conductivity is that of the entire aquifer, K_{11} = 1.90E-05 m/s, and b = 60 meters. T_2 is calculated to be 3.6E+04 m²/yr.

Using Equation 5.2, the drawdown at the well is 58 meters for T_1, and 20 meters for T_2. The actual drawdown is probably between the two values. Using these values as a guideline, s = 25 meters is selected as the drawdown in the well, and the specified head at the well screen is 35 meters. When these values are used in the numerical flow model, the resulting flow to the well matches the selected pumping rate of Q_s = 0.001 m³/s.

The specified head at the water table and at the pumping well screen induces a net inflow through the top of the radial flow model. This net inflow is 0.05 m/yr. This value is less than the assumed recharge of 0.40 m/yr (see Section 2.1) because it is a net value, taking into consideration local discharges along the water table.

The radial model, as compared to the rectangular model, is greater in overall horizontal problem scale by almost an order of magnitude. In Figure 3-3, for an overall problem scale on the order of 10^4 meters, Gelhar (1993) gives a corresponding horizontal correlation scale, λ_1, of 1000 meters, an order of magnitude increase over the value used in the rectangular model. This, in turn, affects the calculation of A_0 in Equation 3.3. Since the radial model has a horizontal extent that is 100 times greater that its vertical extent, the flow is predominantly horizontal. If this is assumed to be the case, in Equation 3.5, θ is expected to be smaller than the value used in the rectangular model. This observation results in a larger value of γ in Equation 3.5. Therefore, even though λ_1 is ten times greater than in the rectangular model, A_0 is not also ten times larger, as a result of the increase in γ (see Equation 3.3). A value of A_0 for the radial model is assumed to be 150 meters. Maintaining the relationship of A_0/A_{33} = 100, A_{33} is assumed to be 1.5 meters. If the macrodispersivity enhancement were evaluated for the radial model, the increased value of γ would affect those results as well.

5.2.2 Results

A simulation of the 2D radial model is performed for an input of tritium as a contaminant. The input concentration for a step input (see Table 4.2) is used for a duration of 600 years, beyond which it is assumed that the inventory is depleted, and no further concentration enters. (see Table 4.1). This input is equivalent to a pulse of 600 years in duration. The other input parameters are the same as those used in the rectangular model, with the exception of those described above in Subsection 5.2.1. The simulation is carried out for 2000 years.

Breakthrough concentrations are measured at the property boundary well, at the river, and at the pumping well (see Figure 5-14 for relative locations). Figures 5-15 and 5-16 show these breakthrough curves. Figure 5-17 displays the contours of concentration in the model cross-section at 605 years, following the depletion of the concentration source. These contours represent the maximum levels of concentration in the simulation. Because the results do not indicate any significant concentration levels at either the river or the pumping well, no additional simulations are performed with this model.

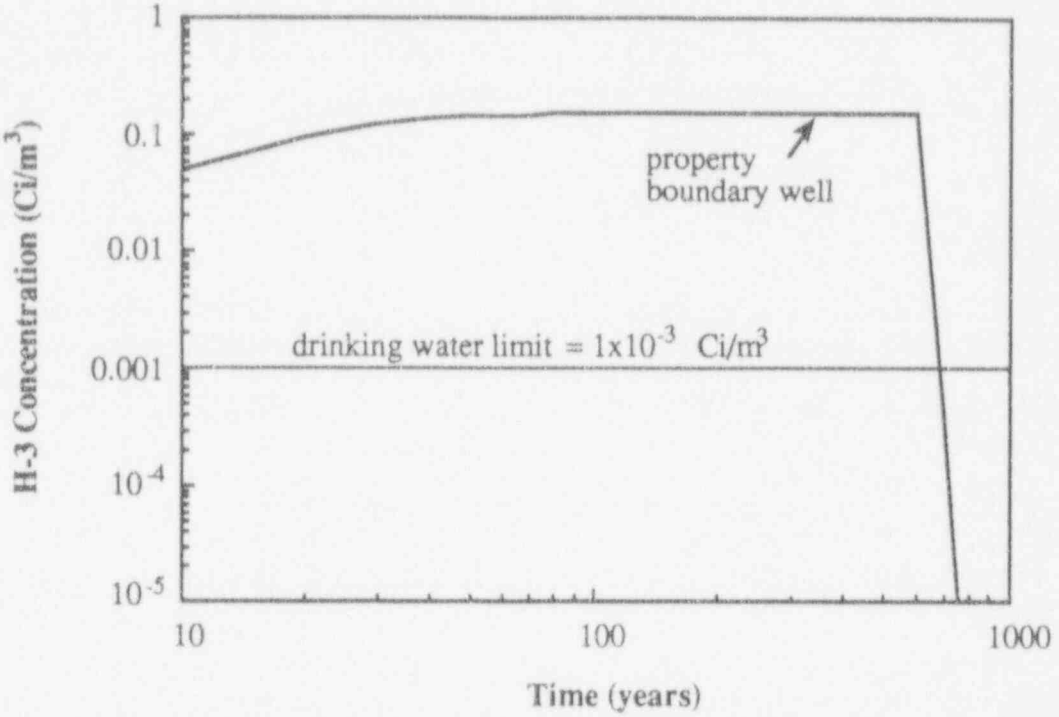

Figure 5-15 Breakthrough concentration curve for tritium at the property boundary well using the 2D radial model.

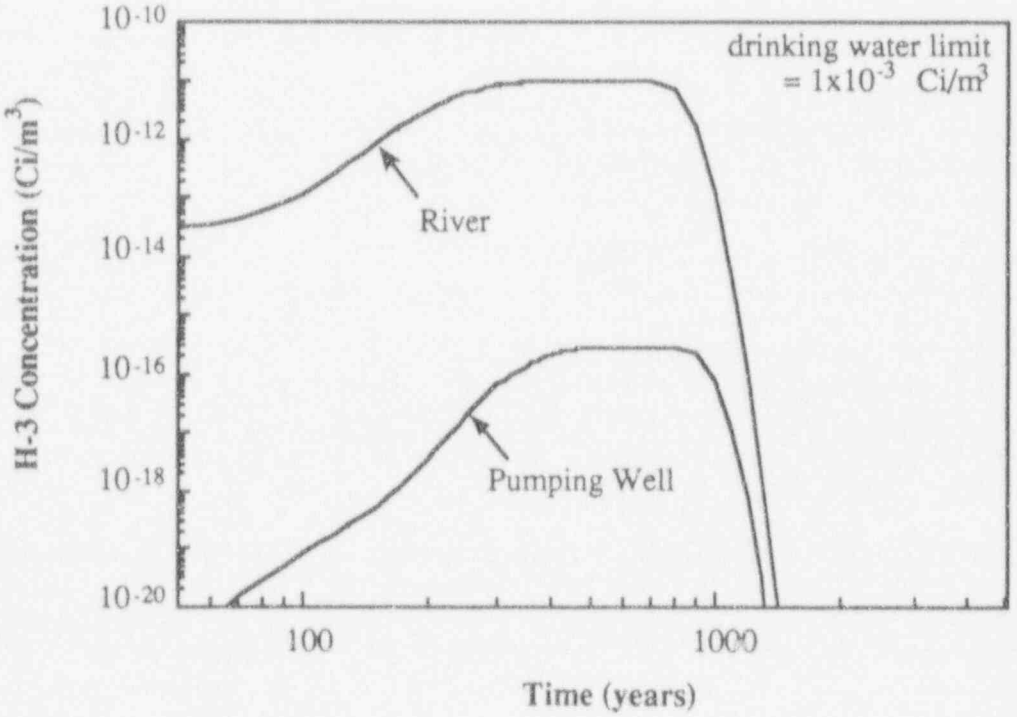

Figure 5-16 Breakthrough concentration curves for tritium at the river and at the pumping well using the 2D radial model.

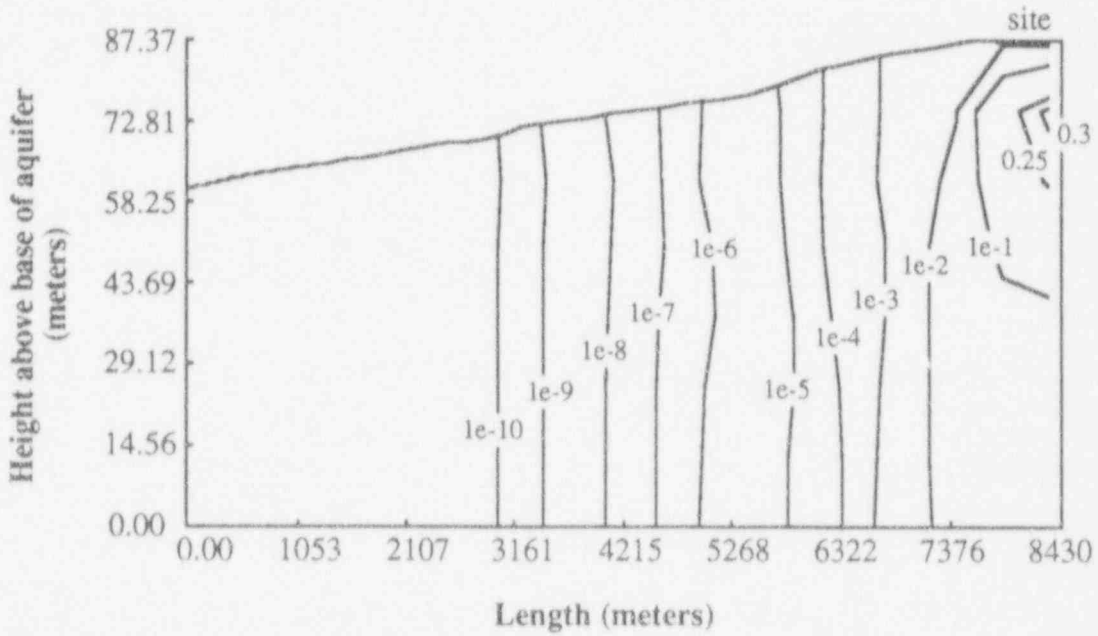

Figure 5-17 Concentration contours of tritium in the 2D radial model cross-section at 605 years. Contours in Ci/m³; vertical scale greatly exaggerated.

5.2.3 Discussion

The results of the radial model indicate that, even with a larger macrodispersivity, tritium contamination does not reach the river or the pumping well in significant quantity. The very low concentration contours shown in Figure 5-17 are insignificant. Kapoor (1993) describes the high uncertainty in predicting concentration values at distances far from the center of a plume. The magnitude of the coefficient of variation of the concentration is very large for distances far from the plume center. Therefore, the low contour lines in Figure 5-17 (1E-7 to 1E-10 Ci/m^3) have virtually no predictive value.

At the property boundary well, the radial model predictions are similar to those predicted by the rectangular model. Because the discretization of the mesh from the site to the property boundary well is much greater in the rectangular model, the radial model results at the property boundary well are a less accurate estimate of concentration.

The distances from the site to the river and to the pumping well are so large that, even for isotopes that do not decay quickly, the expected time for the concentrations to reach significant levels at the pumping well and at the river will be on the order of 10^5 or 10^6 years. Even the isotopes with long half-lives will experience some decay during this time, further reducing the measurable concentrations.

The concentration values in Figures 5-15 and 5-16 for the river and for the pumping well are undiluted concentrations. The effect of dilution at the river from the river streamflow and from other river discharge sources is not taken into consideration. In a similar manner, the contaminated water represents only 15/360 of the flow at the well. The remaining flow contribution would cause notable dilution at the well. These observations, based on the 2D radial model, additionally emphasize that significant contamination at either the river or the pumping well is unlikely.

5.3 Predictions and Uncertainty

In Chapter 4, two screening models are used to evaluate the input contamination. Having used the same isotopes in the numerical models, it is possible to compare the screening model predictions with the rectangular numerical model results at the spring. This comparison shows the sensitivity of the prediction of the contamination to model configuration. Both the results of numerical model and the analytical models have uncertainties associated with the effective mean solutions. An evaluation of these uncertainties is performed, using the analytical pulse screening model as a representative example.

5.3.1 Analytical Predictions of Numerical Results

Step Input

The results of the 1D step model in Chapter 4 are compared to the numerical model results for tritium at the spring in Figure 5-18. A similar comparison is made for uranium-238 in Figure 5-19. As these figures show, for these isotopes the 1D step model tends to overestimate the steady state concentration and to underestimate the travel time. One reason for these differences is that the 1D step model does not take into consideration transverse dispersivity (see Appendix A for a derivation of the 1D model). In the numerical model, transverse dispersivity spreads the plume perpendicular to the flow, resulting in a decrease in peak plume concentration. A second difference in the models is that the travel time for the 1D analytical model is calculated from a single mean

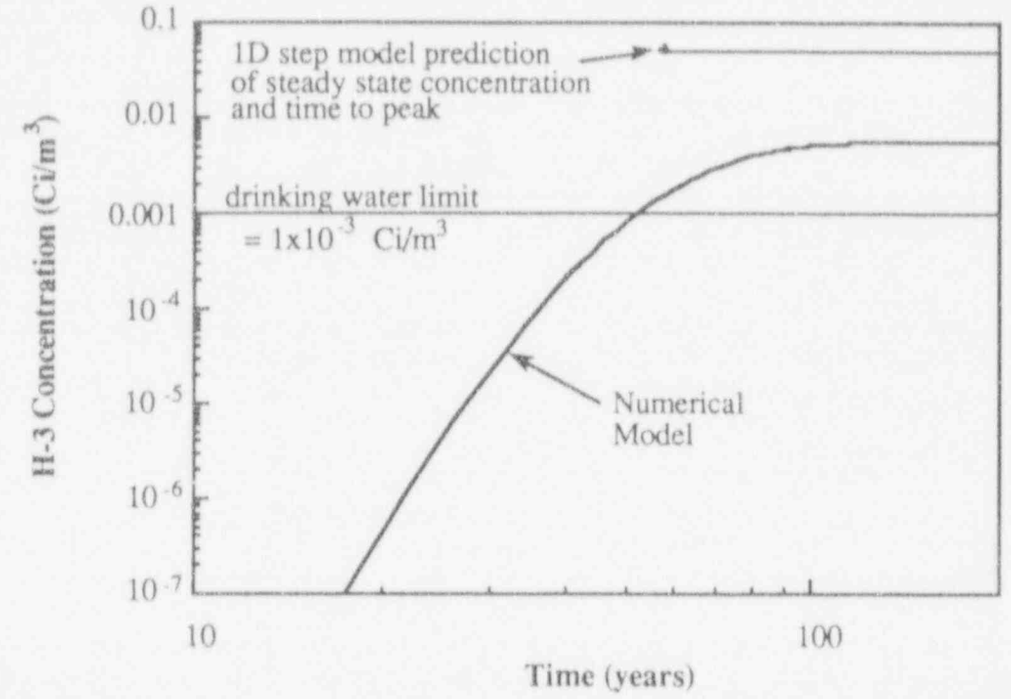

Figure 5-18 Comparison of H-3 concentration breakthrough curves at the spring for the 1D step model prediction and for the 2D rectangular numerical simulation.

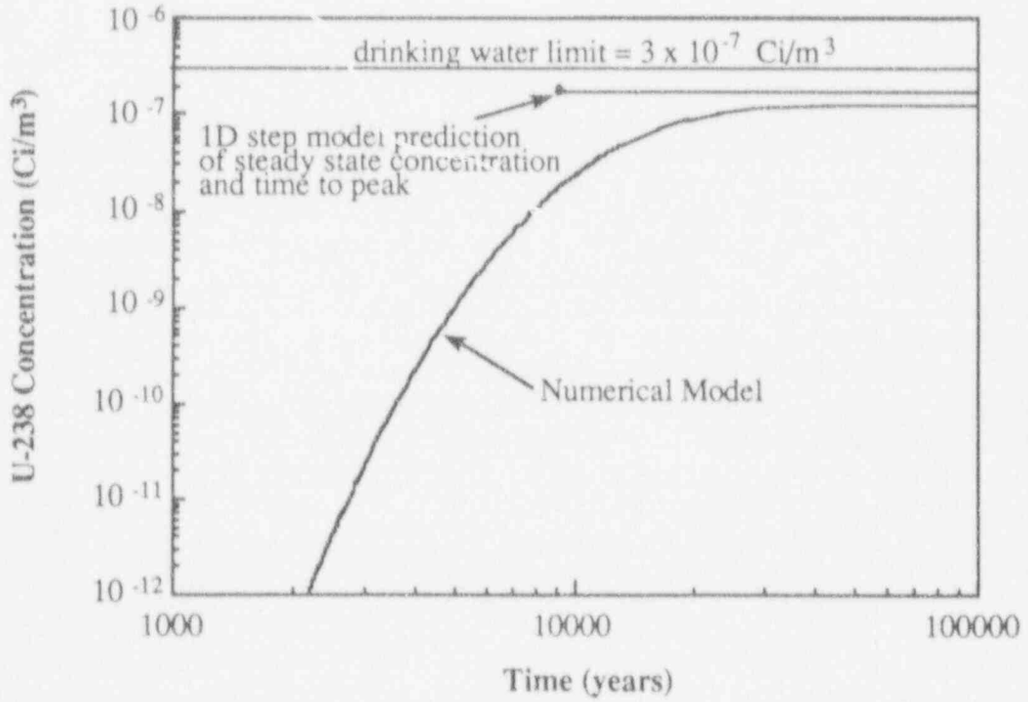

Figure 5-19 Comparison of U-238 concentration breakthrough curves at the spring for the 1D step model prediction and for the 2D rectangular numerical simulation.

flow velocity. The velocity flow field in the numerical model varies spatially in magnitude and in direction.

The spatial description of the source concentration is a third difference between the two types of models. The 1D analytical model assumes a point source with a uni-directional velocity. The numerical model employs a distributed source concentration in a varying velocity field. As a result, in the numerical model the contaminant moves in different streamtubes and arrives at the spring over a range of time. The time for the numerical model concentration to reach the steady state concentration level at the spring is therefore controlled by the travel time of the contamination in the streamtube with the longest travel distance. In general, despite minor differences, for both isotopes the 1D step model is a reasonable predictor of both magnitude and timing.

It is important to recognize that, while the 1D step model solution appears to offer a conservative prediction of the numerical solution for H-3 and for U-238, for isotopes with high macrodispersivities and short half-lives it may not show the same relationship to the numerical solution. Further work in this area would include an analysis of isotopes that exhibit this behavior and that may be modeled by a step input.

Pulse Input

Figure 5-20 is a comparison of the 2D analytical pulse prediction and the 2D numerical model results for strontium-90 (see Appendix B for a detailed discussion of the 2D analytical solution). Figure 5-21 is a similar comparison for technetium-99. In both cases, in comparison to the numerical solution, the pulse model underestimates the concentration at early times and underestimates the peak concentration.

A major difference between the two isotope examples is that for strontium-90 the 2D pulse solution predicts a longer time to peak than does the numerical model, while for technetium-99 it predicts a shorter time to peak. This difference can be explained by the short half-life of Sr-90 and the extremely long half-life of Tc-99 in the following discussion. Like the 1D step solution, the 2D pulse solution assumes a uni-directional constant velocity. As discussed above, the numerical model experiences a spatially-varying velocity. This velocity variation results in an effective longitudinal dispersion, compounded by the local circulation in the different streamtubes. For an isotope with a short half-life and a high dispersivity, more of the undecayed isotope species will reach far distances in the aquifer at early times. Because of the short half-life, in the increased time it takes the edge of the plume in the 2D pulse model to reach the same distance as that of the numerical model, the isotope will experience significant decay. Therefore at early times, the difference between the uniform velocity 2D pulse model and the numerical model will be great.

This non-uniform flow is also the reason why, for strontium-90, the time to the peak measured concentration in the numerical model is shorter than the time to the peak for the 2D pulse model. It is not that the peaks arrive at different times, it is that the measurements of undecayed concentration in advance of the center of the plume have the effect of "moving" the numerical plume peak higher in magnitude and forward in time. When the peaks pass, the two solutions converge as the diluted concentrations decrease, and the decay continues.

Because the half-life of technetium-99 is very long, it represents the case of a non-decaying contaminant. The non-uniform velocity is still the cause of an increased spreading of the numerical model plume, but the lack of decay results in a solution of the analytical model that is much closer to that of the numerical model at early time. Because the isotope does not decay, the spreading of contaminant in advance of the peak

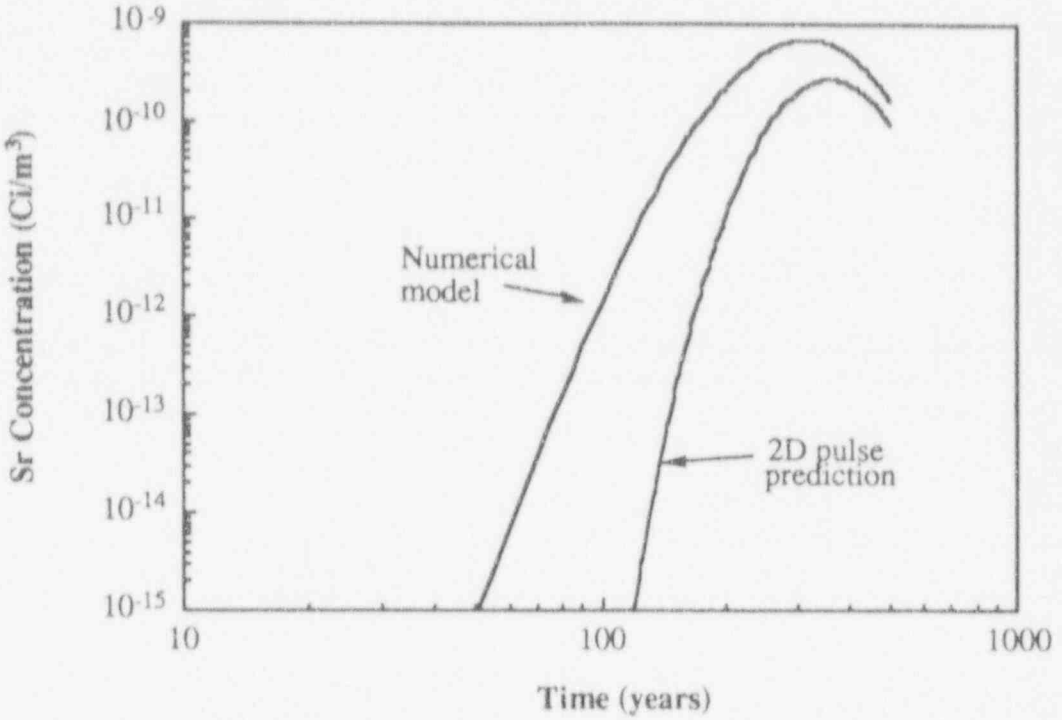

Figure 5-20 Comparison of Sr-90 concentration breakthrough curves at the spring for the 2D pulse model prediction and for the 2D rectangular numerical simulation.

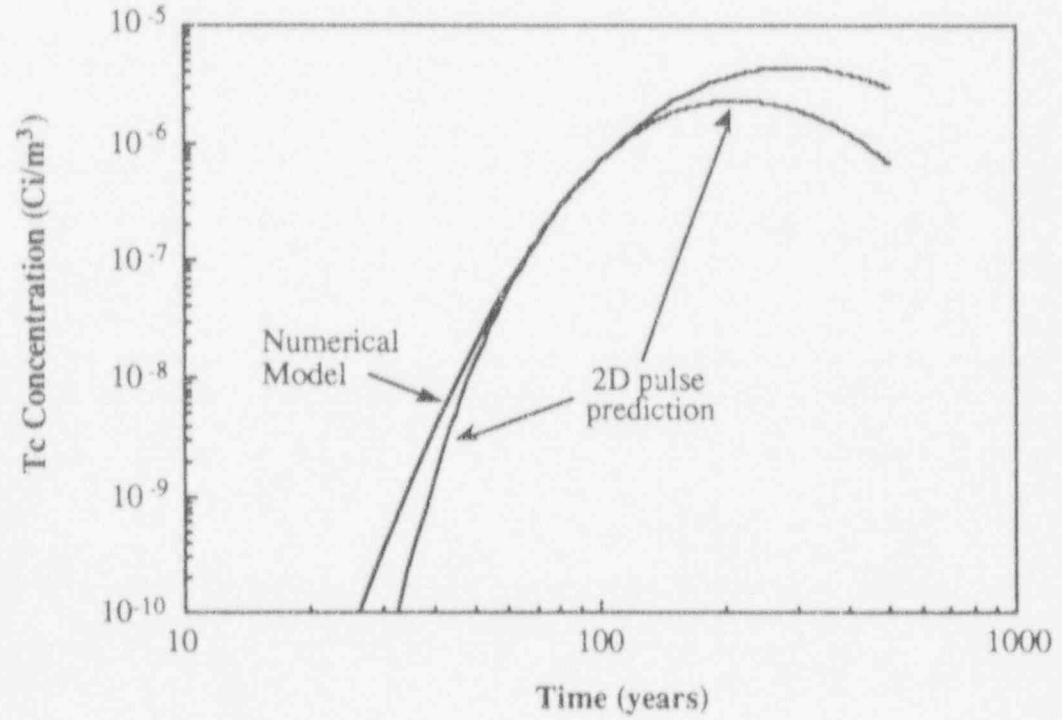

Figure 5-21 Comparison of Tc-99 concentration breakthrough curves at the spring for the 2D pulse model prediction and for the 2D rectangular numerical simulation.

will not affect the measured location of the peak. Other issues, such as model configuration as described above for the step solution, may provide an explanation for the differences in peak magnitude and timing between the two models of Tc-99. In general, however, the pulse model offers a reasonable prediction of the concentration breakthrough curves.

5.3.2 Uncertainties in Model Predictions

The discussion in Subsection 5.3.1 illustrates the sensitivity of the concentration predictions to analytical and numerical model assumptions. Regardless of the model configuration, the concentration predictions in all the models are mean, or effective, solutions. The sensitivity of the predictions to various parameters highlights the potential sources of uncertainty in the mean solution. Model configuration, as discussed in Subsection 5.3.1, is one source of uncertainty. The mean solutions are based on effective flow and transport input parameters that are derived in the manner discussed in Chapter 3. Inadequate estimates of these effective parameters are another source of uncertainty in the mean solution. Another aspect of uncertainty concerns the variations of concentration around the mean solution as a result of heterogeneity. Some theoretical approaches to predicting these variations of concentration around the mean are discussed in Gelhar (1993, section 5.3).

Uncertainties in the mean solution

The sensitivity of the model predictions to uncertainties in the effective parameters is demonstrated using the pulse screening model from Section 4.1 for strontium-90 at the spring. Figure 5-22 contrasts the behavior of the pulse model with an enhanced longitudinal macrodispersivity (A_{11} = 242m) with that of an unenhanced macrodispersivity (A_{11} = 25m). The first case corresponds to heterogeneous sorption, and the second case corresponds to a non-sorbing solute. In modeling groundwater transport, it is common practice to arbitrarily assume the same unenhanced dispersivity for all transported species. The results in Figure 5-22 show that this assumption can yield extreme underestimates of peak concentration (by 10 orders of magnitude). This same extreme difference in magnitude of the peak concentration is found using the numerical model (see Figure 5-13).

The sensitivity of the screening model is further illustrated in Figure 5-22 by considering the influence of a 25 percent increase in the longitudinal dispersivity and a 25 percent decrease in the retardation factor. This modest change in these key input parameters produces an increase in the peak concentration of two orders of magnitude. Overall, these sensitivity results emphasize the importance of reliable dispersivity estimates, especially in cases of radionuclides with small half-lives (28.8 years for strontium-90) compared to the retarded mean travel time (3400 years for strontium-90) (see also Section 5.3.1).

Uncertainties around the mean solution

The variations in concentration around the mean concentration can be characterized through a stochastic evaluation of the concentration variance. The stochastic theory has been developed for the case of saturated transport of non-sorbing solutes by Vomvoris and Gelhar (1990) and Kapoor (1993). For purposes of qualitative illustration, it will be assumed that the developed theory for a non-sorbing solute is applicable to the case with spatially variable sorption, provided that the enhanced macrodispersivity is used for the sorbing species. Kapoor (1993, equation 3.28) shows that after relatively

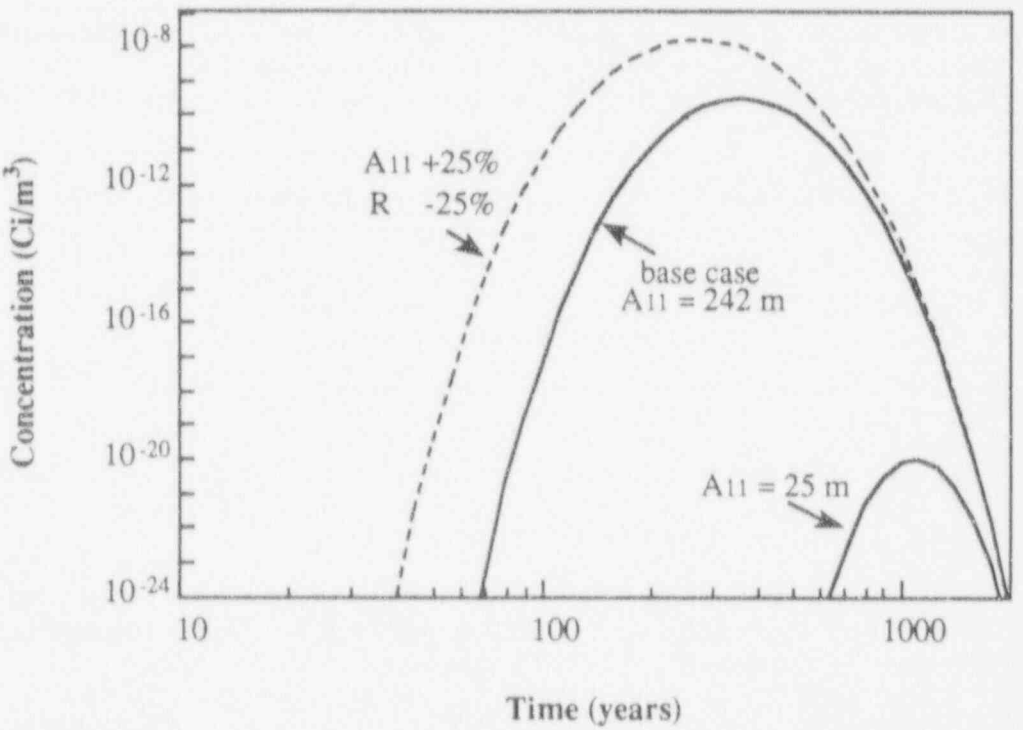

Figure 5-22 Sensitivity of the 2D pulse screening model for strontium-90 to changes in input parameters.

large plume displacement the concentration variance along the centerline of the plume can be approximated by

$$\sigma_C^2 = \frac{2A_{11}\hat{v}}{\chi}\left(\frac{\partial \overline{C}}{\partial x}\right)^2 \tag{5.3}$$

where $\overline{C}$ is the mean concentration, x is the longitudinal distance, A_{11} is the longitudinal macrodispersivity, $\hat{v}$ is the retarded velocity, and χ is a rate constant for variance decay that depends on the microscale of the velocity variations. Equation 5-3 is a local variance relationship indicating that the concentration variance is proportional to the square of the mean concentration gradient. This equation is applicable everywhere along the centerline of the plume, except very near the point of maximum mean concentration where the gradient is zero. At that location a modified form, as developed by Kapoor (1993), is applicable.

The coefficient of variation of concentration can be expressed from Equation 5.3 as

$$\frac{\sigma_C}{\overline{C}} = L\left|\frac{\partial \ln \overline{C}}{\partial x}\right| = \frac{L|x-\hat{v}t|}{2A_{11}\hat{v}t} \tag{5.4}$$

where L is given by

$$L = \left(\frac{2A_{11}\hat{v}}{\chi}\right)^{1/2} \tag{5.5}$$

Equation 5.4 is found by differentiating the expression for the two-dimensional pulse solution (Equation 4.7) evaluated on the centerline of the plume ($z = 0$). The parameter L is evaluated using the results in Kapoor (1993, appendix IV), assuming that the microscales of $\ln K$ are one tenth of the correlation scales, and that the local longitudinal and transverse dispersivities are 0.005 m and 0.0005 m, respectively. Using the resulting value of L = 409 m, the expected variation of concentration is evaluated for the strontium-90 breakthrough at the spring as shown in Figure 5.23. The mean concentration is the solid line, and the mean plus two standard deviations is the dashed line in Figure 5-23. This calculation indicates that the variation of concentration around the mean can be very large. Concentration fluctuations reflecting the effect of aquifer hydraulic and chemical heterogeneity can produce concentrations as much as two orders of magnitude larger than the mean predicted by a traditional deterministic analytical or numerical solution. Because the currently available theory does not explicitly consider the effects of heterogeneous sorption, this theoretical evaluation of the concentration variance should be regarded as tentative.

In summary, the concentration predictions are subject to uncertainties in the mean solution and to uncertainties around the mean solution. Consequently, the results of the transport simulations should be regarded as crude order of magnitude estimates. The results are particularly sensitive to the magnitude of the dispersivity for the sorbing solutes. Major improvements in the reliability of the predictions could be attained if systematic data on the variation of sorption characteristics and their correlation with hydraulic conductivity were obtained.

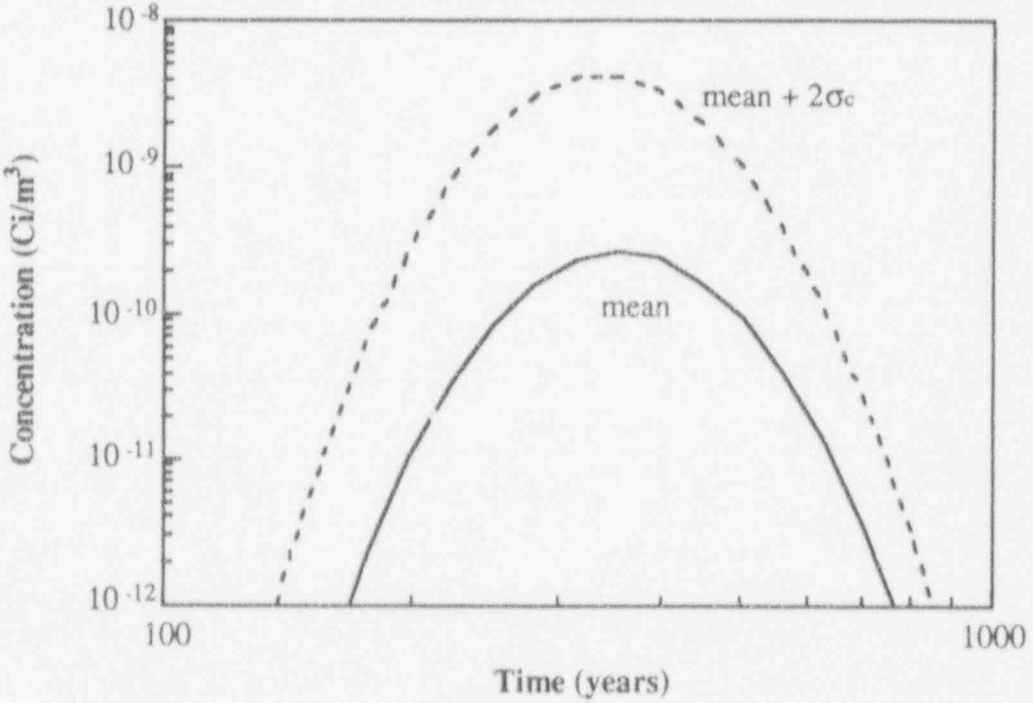

Figure 5-23 Mean concentration (solid line) plus two standard deviations (dashed line) for strontium-90 at the spring, using the 2D pulse screening model.

CHAPTER 6
CONCLUSIONS AND RECOMMENDATIONS

6.1 Conclusions

This report demonstrates the application of stochastic parameter estimation to a hypothetical LLW site. Drawing upon the type of site data sources that are commonly available, stochastic theory is used to systematically derive input parameters for a traditional flow and transport numerical model. A unique feature of this report is that it uses standard data sources and a commercially-available numerical model, but it defines a new methodology of parameter derivation based on stochastic principles. The step-by-step application of this methodology in the preceding chapters confirms the viability of this approach to modeling LLW sites.

The results of the stochastic parameterization process are mean or effective hydraulic parameters that are sensitive to site variables. The effective parameters are used in numerical and analytical algorithms to determine mean concentration predictions. Sensitivities to effective input parameters and to model configurations contribute to uncertainty in the mean predictions. Additionally, since the effective concentration predictions represent a mean solution, fluctuations about this mean are another source of uncertainty. These uncertainties are also present in traditional parameter estimation methods, where they are often unnoticed and incalculable. The effect of the uncertainty in the concentration predictions is that they represent a band of estimates over a range of at least an order of magnitude. Any conclusions drawn from the predictions must take into consideration their approximate nature.

An outcome of the stochastic parameter estimation process is the use of species-dependent enhanced longitudinal macrodispersivities in the numerical and analytical models. It is common practice in traditional models to use the same macrodispersivity for all species. The analysis in this report shows the importance of varying macrodispersivity by contaminant species on the basis of sorption heterogeneity and correlation with hydraulic conductivity. An enhancement of macrodispersivity is shown to have enormous effects on the expected concentration predictions for both numerical and analytical models. This is seen as particularly important for isotopes that have a short half-life relative to their retarded mean travel time.

Concentration and peak time predictions of one-dimensional (1D) and two-dimensional (2D) analytical models are compared to the numerical model results and are found to give reasonable peak estimates. However, the overall shapes of the analytical breakthrough curves tend to underestimate numerical concentration results, especially for early times. On the basis of these findings, it is concluded that while they are useful for screening the input isotopes, the 1D and 2D analytical uniform flow models can not adequately treat the complicated flow system as represented by the 2D cross-section in the numerical model.

6.2 Recommendations

Because the magnitude of the macrodispersivity enhancement has significant effects on concentration output, it is important to be able to make accurate estimates of this input parameter. Macrodispersivity enhancement, as a function of sorption variability and correlation with hydraulic conductivity, needs to be quantified for each contaminant species. It is therefore important to emphasize the recommendation that, in the data collection process, measurements of the sorption distribution coefficient (K_d) for each species should be made on the same soil samples as are measurements of hydraulic conductivity (K). From these measurements, a direct correlation of K and K_d may be derived for each species. Because it is not yet common practice to perform stochastic parameter estimation, this correlation is normally not developed explicitly. As this approach becomes more widely used, the necessity of measuring K and K_d correlation will be recognized.

An analysis of unsaturated zone flow and transport was not included in this report. The effect of excluding the unsaturated zone at humid sites is a subject for future analysis. Additionally, it is recommended that this modeling approach be applied to arid sites, with the inclusion of unsaturated zone stochastic theory for the estimation of unsaturated parameters. As explored for the saturated zone in this report, analytical and numerical model predictions and sensitivities could be compared for the unsaturated zone.

Based on the findings of substantial differences between the 1D analytical and 2D numerical solutions, it may be worthwhile to evaluate a 3D model in a future project. Similarly, other 2D model configurations could be explored. A 2D model with a larger spatial extent, or one that incorporates temporal or spatial variations in the contamination source are important options for future consideration.

The uncertainties in the analytical and numerical model results are investigated to an extent in this report, but a more comprehensive evaluation of the different aspects needs to be made. This analysis would include a development of the stochastic theory of concentration variance around the mean concentration solution for solutes with spatially-variable sorption. Additionally, in applying these modeling techniques to an actual site, the concentration predictions would be validated through a comparison with field concentration measurements. This point further emphasizes the need for better cooperation between the groundwater modeling goals and the plans for measuring field data at the site. Even if it is not achieved to a full extent, any improvement in this cooperation will greatly increase the effectiveness of the stochastic parameter estimation process.

REFERENCES

Cahill, J.M., *Hydrology of the low-level radioactive solid-waste burial site and vicinity near Barnwell, South Carolina*, U.S. Geological Survey Open File Report 82-863, 1982.

Campbell, A. C., *Geochemistry of soils and waters at LLW disposal site*, U.S. Nuclear Regulatory Commission Staff Report, 1992.

Dennehy, K.F. and P.B. McMahon, *Water movement in the unsaturated zone at a low-level radioactive waste burial site near Barnwell, South Carolina*, U.S. Geological Survey Open File Report 87-46, 1987.

Garabedian, S.P., L.W. Gelhar, and M.A. Celia, *Large-scale dispersive transport in aquifers: field experiments and reactive transport theory*, R.M. Parsons Lab Tech. Report No. 315, Massachusetts Institute of Technology, Cambridge, MA, 1988.

Gelhar, L.W. and C.L. Axness, Three-dimensional stochastic analysis of macrodispersion in Aquifers, *Water Resources Research*, 19(1), 161-180, 1983.

Gelhar, L.W., C. Welty, and K.R. Rehfeldt, a critical review of data on field-scale dispersion in aquifers, *Water Resources Research*, 28(7), 1955-1974, 1992.

Gelhar, L.W., *Stochastic Subsurface Hydrology*, Prentice Hall, New York, 1993.

Gelhar, L.W., Stochastic subsurface hydrology from theory to applications, *Water Resources Research*, 22(9), 135s-145s, 1986.

Goode, D.J., *Nonradiological groundwater quality at low-level radioactive waste disposal sites*, Technical Report No. NUREG-1183, U.S. Nuclear Regulatory Commission, 1986.

Hoeffner, S.L., *Radioactive sorption on Savannah River Plant burial ground soil – A summary and interpretation of laboratory data*, DP-1702, E.I. du Pont de Nemours & Co., Savannah River Laboratory, Aiken, SC, 1985.

Kapoor, V., *Macrodispersion and concentration fluctuations in three-dimensionally heterogeneous aquifers*, ScD dissertation, Massachusetts Institute of Technology, Cambridge, MA, 1993.

Mantoglou, A. and L.W. Gelhar, Effective hydraulic conductivities of transient unsaturated flow in stratified soils, *Water Resources Research*, 23(1), 57-67, 1987a.

Mantoglou, A. and L.W. Gelhar, Stochastic modeling of large-scale transient unsaturated flow systems, *Water Resources Research*, 23(1), 37-46, 1987b.

Phillips, K.J., and L.W. Gelhar, Contaminant transport to deep wells, *Journal of the Hydraulics Division*, ASCE, 104(HY6), 807-819, 1978.

Pietrzak, R.F. and R. Dayal, *Evaluation of isotope migration-land burial. Water chemistry at commercially operated low-level radioactive waste disposal sites. Quarterly Progress Report. October-December 1981*, Report No. NUREG/CR-2192, I(3-4), Brookhaven Nat'l Lab, 1982.

Polmann, D. J., D. McLaughlin, S. Luis, L.W. Gelhar, and R. Ababou, Stochastic modeling of large-scale flow in heterogeneous unsaturated soils, *Water Resources Research*, 27(7), 1447-1458, 1991.

Polmann, D.J., *Application of stochastic methods to transient flow and transport in heterogeneous unsaturated soils*, PhD dissertation, Massachusetts Institute of Technology, Cambridge, MA, 1990.

Polmann, D.J., E.G. Vomvoris, D. McLaughlin, E.M. Hammick, and L.W. Gelhar, *Application of stochastic methods to the simulation of large-scale unsaturated flow and transport*, Report No. NUREG/CR-5094, U.S. Nuclear Regulatory Commission, 1988.

Rehfeldt, K.R., and L.W. Gelhar, Stochastic analysis of dispersion in unsteady flow in heterogeneous aquifers, *Water Resources Research*, 28(8), 2085-2099, 1992.

Vomvoris, E.G., and L.W. Gelhar, Stochastic analysis of the concentration variability in a three-dimensional, heterogeneous aquifer, *Water Resources Research*, 26(10), 2591-2602, 1990.

Voss, C.I., *A finite-element simulation model for saturated-unsaturated, fluid-density-dependent groundwater flow with energy transport or chemically-reactive single-species solute transport*, USGS Water Resources Investigations Report 84-4369, 1984.

Yeh, T.-C., L.W. Gelhar, and A.L. Gutjahr, Stochastic analysis of unsaturated flow in heterogeneous soils, 1., Statistically isotropic media, *Water Resources Research*, 21(4), 447-456, 1985.

APPENDIX A
ONE-DIMENSIONAL STEP INPUT SOLUTION

The following is a derivation of the 1D step input solution as used in Subsection 4.1.1. It is analagous to a 1D column experiment with a steady-state concentration release at the top of the column.

The 1D form of the advection-dispersion equation with decay and retardation is given by:

$$R\frac{\partial C}{\partial t} + v\frac{\partial C}{\partial x} - A_{11}v\frac{\partial^2 C}{\partial x^2} + RCk = 0 \qquad \text{(A.1)}$$

where x is the horizontal distance, k is the decay coefficient, R is the retardation factor, C is the steady-state concentration, v is the fluid velocity, and A_{11} is the longitudinal macrodispersivity. Let $\hat{v} \equiv v/R$, and assuming steady state, $\partial C/\partial t = 0$. Then:

$$\frac{\partial C}{\partial x} - A_{11}\frac{\partial^2 C}{\partial x^2} + \frac{Ck}{\hat{v}} = 0 \qquad \text{(A.2)}$$

Multiplying through by $\hat{v}/k$, and letting $\hat{x} = (xk)/\hat{v}$ and $\partial\hat{x} = \partial x(k/\hat{v})$ gives:

$$\frac{\partial C}{\partial \hat{x}} - \frac{kA_{11}}{\hat{v}}\frac{\partial^2 C}{\partial \hat{x}^2} + C = 0 \qquad \text{(A.3)}$$

if B is defined as $B = (kA_{11})/\hat{v}$, then Equation A.3 may be written as:

$$-B\frac{\partial^2 C}{\partial \hat{x}^2} + \frac{\partial C}{\partial \hat{x}} + C = 0 \qquad \text{(A.4)}$$

Equation A.4 is a second-order homogeneous differential equation. Substituting $C = \exp(m\hat{x})$ gives the characteristic form of the equation to be:

$$-Bm^2 + m + 1 = 0 \qquad \text{(A.5)}$$

where m is a root of Equation A.5, and $C = \exp(m\hat{x})$ is a solution of Equation A.3. Solving the quadratic in Equation A.5 for m, and satisfying the initial conditions, at $x = 0$, $C(x) = C_0$, the solution is given by:

$$C(\hat{x}) = C_0 \exp(+m\hat{x}) \qquad \text{(A.6)}$$

where C_0 is the initial source concentration. Substituting back in for m and for $\hat{x}$, and rearranging:

$$C = C_0 \exp\left[-\left(\frac{-1+\sqrt{1+4B}}{2A_{11}}\right)x\right] \tag{A.7}$$

Let

$$\kappa = \frac{-1+\sqrt{1+4B}}{2A_{11}} \tag{A.8}$$

then

$$C(x) = C_0 e^{-\kappa x} \tag{A.9}$$

which corresponds to Equation 4.2. $C(x)$ is the steady-state concentration.

The 1D step input solution is applicable to those isotopes that have a relatively low solubility in comparison to their site inventory. H-3 and U-238 are evaluated using this method in Subsection 4.1.1.

APPENDIX B
TWO-DIMENSIONAL PULSE INPUT SOLUTION

The following is a derivation of the 2D pulse input solution as used in Subsection 4.1.2.

The 2D form of the advection-dispersion equation with uniform horizontal velocity, first-order decay, and retardation is:

$$R\frac{\partial C}{\partial t} + v\frac{\partial C}{\partial x} - A_{11}v\frac{\partial^2 C}{\partial x^2} - A_{33}v\frac{\partial^2 C}{\partial z^2} + RCk = 0 \qquad \text{(B.1)}$$

where x is the horizontal direction, z is the vertical distance as measured from the center of the plume, t is the time after the pulse is released, k is the decay coefficient, R is the retardation factor, C is the steady-state concentration, v is the fluid velocity, A_{33} is the vertical transverse macrodispersivity, and A_{11} is the longitudinal macrodispersivity. Let $\hat{v} \equiv v/R$, then:

$$\frac{1}{\hat{v}}\frac{\partial C}{\partial t} + \frac{\partial C}{\partial x} - A_{11}\frac{\partial^2 C}{\partial x^2} - A_{33}\frac{\partial^2 C}{\partial z^2} + \frac{Ck}{\hat{v}} = 0 \qquad \text{(B.2)}$$

Equation B.2 is a second-order homogeneous partial differential equation that may be solved for $C(x, z, t)$. For a pulse input of mass, M, over a width, w, in the unidirectional velocity field, the solution is given by:

$$C(x,z,t) = \frac{M \exp\left\{-\left[\frac{(x-\hat{v}t)^2}{4A_{11}\hat{v}t} + \frac{z^2}{4A_{33}\hat{v}t} + kt\right]\right\}}{R\ n\ w\ 4\pi\ \hat{v}t\ \sqrt{A_{11}A_{33}}} \qquad \text{(B.3)}$$

where n is the porosity. The maximum value of C at a particular downstream distance x for any time will be at the center of the plume, where $z = 0$. Letting $\beta = Rnw4\pi\hat{v}$ the maximum value of C is given by:

$$C(x,t) = \frac{M \exp\left\{-\left[\frac{(x-\hat{v}t)^2}{4A_{11}\hat{v}t} + kt\right]\right\}}{\beta t\ \sqrt{A_{11}A_{33}}} \qquad \text{(B.4)}$$

At any location x, the maximum value of $C(x,t)$ will occur at some peak time, t_p.

$$C_{max}(x) = \max\left\{\frac{Me^{-kt}}{t\beta\sqrt{A_{11}A_{33}}}\exp\left[-\frac{(x-\hat{v}t)^2}{4\hat{v}tA_{11}}\right]\right\} = C(x,t_p) \qquad \text{(B.5)}$$

Equation B.5 corresponds to Equation 4.7 in Subsection 4.1.2.

The peak time, t_p, is found by taking the natural logarithm of Equation B.5, by differentiating it with respect to time, and by setting it equal to zero. Let $\hat{t} = (\hat{v}t)/x$, $N = (kx)/\hat{v}$, and $P = (4A_{11})/x$. Taking the natural logarithm of Equation B.5:

$$\ln(C_{max}) = \ln\left(\frac{M\hat{v}}{x\beta\sqrt{A_{11}A_{33}}}\right) - \ln\hat{t} - N\hat{t} - \frac{(1-\hat{t})^2}{P\hat{t}} \qquad \text{(B.6)}$$

Differentiating with respect to $\hat{t}$:

$$0 = -\frac{1}{\hat{t}} - N + \frac{2(1-\hat{t})}{P\hat{t}} + \frac{(1-\hat{t})^2}{P\hat{t}^2} \qquad \text{(B.7)}$$

multiplying through by $P\hat{t}^2$ gives:

$$0 = -P\hat{t} - NP\hat{t}^2 + 2\hat{t}(1-\hat{t}) + (1-\hat{t})^2 \qquad \text{(B.8)}$$

Expanding and collecting like terms gives a quadratic

$$0 = \hat{t}^2(1 + NP) + \hat{t}(P) - 1 \qquad \text{(B.9)}$$

The expression in Equation B.9 may be solved using the quadratic formula. Solving and rearranging gives:

$$\hat{t} = \frac{-1 + \sqrt{1 + \frac{4}{P}\left(N + \frac{1}{P}\right)}}{2\left(N + \frac{1}{P}\right)} \qquad \text{(B.10)}$$

Substituting back in the expressions for N, P, and $\hat{t}$, the final solution for t_p is:

$$t_p = \frac{-1 + \sqrt{1 + \frac{x^2}{\hat{v}A_{11}}\left(k + \frac{\hat{v}}{4A_{11}}\right)}}{2\left(k + \frac{\hat{v}}{4A_{11}}\right)} \qquad \text{(B.11)}$$

Equation B.11 is the same as Equation 4.8. The pulse input solution is applicable to those isotopes that have a high solubility relative to their site inventory. Sr-90 and Tc-99 are evaluated using this method in Subsection 4.1.2.

NRC FORM 335 (2-89) NRCM 1102, 3201, 3202

U.S. NUCLEAR REGULATORY COMMISSION

BIBLIOGRAPHIC DATA SHEET

(See instructions on the reverse)

1. REPORT NUMBER (Assigned by NRC. Add Vol., Supp., Rev., and Addendum Numbers, if any.)
NUREG/CR-6114
Vol. 3

2. TITLE AND SUBTITLE
Performance Assessment of a Hypothetical Low-Level Waste Facility

Groundwater Flow and Transport Simulation

3. DATE REPORT PUBLISHED
MONTH: May
YEAR: 1994

4. FIN OR GRANT NUMBER
D2044

5. AUTHOR(S)
M. E. Talbott, L. W. Gelhar

6. TYPE OF REPORT
technical

7. PERIOD COVERED *(Inclusive Dates)*

8. PERFORMING ORGANIZATION – NAME AND ADDRESS *(If NRC, provide Division, Office or Region, U.S. Nuclear Regulatory Commission, and mailing address; if contractor, provide name and mailing address.)*

Ralph M. Parsons Laboratory
Department of Civil and Environmental Engineering
Massachusetts Institute of Technology
Cambridge, MA 02139

9. SPONSORING ORGANIZATION – NAME AND ADDRESS *(If NRC, type "Same as above"; if contractor, provide NRC Division, Office or Region, U.S. Nuclear Regulatory Commission, and mailing address.)*

Division of Regulatory Applications
Office of Nuclear Regulatory Research
U. S. Nuclear Regulatory Commission
Washington, D. C. 20555-0001

10. SUPPLEMENTARY NOTES

11. ABSTRACT *(200 words or less)*

Stochastic subsurface hydrologic theory is applied to data for a hypothetical low-level waste site to demonstrate the features of the hydraulic parameter estimation process, as developed by Gelhar and others. Effective values of hydraulic conductivity, macrodispersivity, and macrodispersivity enhancement are estimated from the data in this manner. A two-dimensional saturated flow and transport finite-element computer code is used to model the site. Four different isotope inputs and two types of input configurations contribute to an evaluation of model sensitivities. These sensitivities of the mean concentrations and the uncertainties around the mean are explored using an analytical model as an example. Results indicate that the spatial heterogeneity of isotope sorption, through its contribution to longitudinal dispersivity enhancement, has a large effect on the magnitude of concentration predictions, especially for isotopes with short half-lives in comparison to their retarded mean travel times. This observation indicates the need for accurate site data measurements that compliment the parameter estimation process. A comparison of simplified analytical screening models with the numerical model predictions shows that the analytical models tend to underestimate concentration levels at low times, potentially as a result of oversimplification of the flow field. Future models could address aspects that are neglected in this report, such as three-dimensionality or unsaturated flow and transport.

12. KEY WORDS/DESCRIPTORS *(List words or phrases that will assist researchers in locating the report.)*
low-level radioactive waste
groundwater model
stochastic
saturated flow
transport
numerical modeling

13. AVAILABILITY STATEMENT
Unlimited

14. SECURITY CLASSIFICATION
(This Page)
Unclassified
(This Report)
Unclassified

15. NUMBER OF PAGES

16. PRICE

Federal Recycling Program